SMC motor proteins extrude DNA asymmetrically and can switch directions

Barth, Roman; Davidson, Iain F.; van der Torre, Jaco; Taschner, Michael; Gruber, Stephan; Peters, Jan Michael; Dekker, Cees

DOI
10.1016/j.cell.2024.12.020

Publication date
2025

Document Version
Final published version

Published in
Cell

Citation (APA)
Barth, R., Davidson, I. F., van der Torre, J., Taschner, M., Gruber, S., Peters, J. M., & Dekker, C. (2025). SMC motor proteins extrude DNA asymmetrically and can switch directions. *Cell*, *188*(3), 749-763. https://doi.org/10.1016/j.cell.2024.12.020

Cell

Article

SMC motor proteins extrude DNA asymmetrically and can switch directions

Graphical abstract

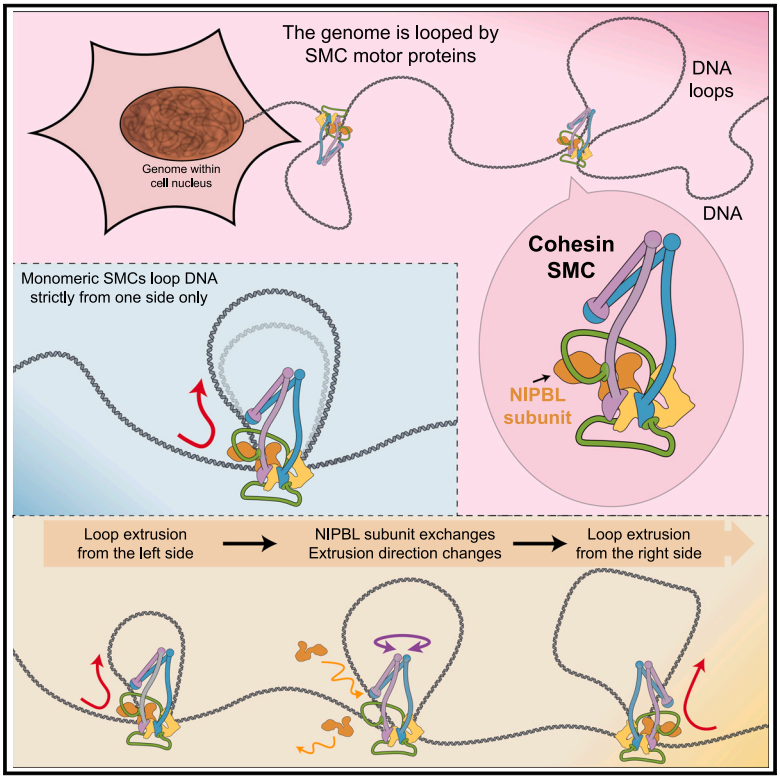

Highlights

- All eukaryotic SMC complexes extrude DNA asymmetrically
- Apparent "symmetric" loop extrusion is the result of frequent direction switches
- On human cohesin, loop-extrusion direction switches require an exchange of NIPBL
- Loop extrusion by cohesin is interspersed with loop diffusion and slipping phases

Authors

Roman Barth, Iain F. Davidson, Jaco van der Torre, Michael Taschner, Stephan Gruber, Jan-Michael Peters, Cees Dekker

Correspondence

c.dekker@tudelft.nl

In brief

All eukaryotic SMC motor proteins extrude DNA asymmetrically but may undergo direction switches, suggesting a common loop extrusion mechanism among all eukaryotic SMC proteins while permitting bidirectional DNA loop extrusion.

Barth et al., 2025, Cell *188*, 749–763
February 6, 2025
https://doi.org/10.1016/j.cell.2024.12.020

CellPress

Cell

CellPress
OPEN ACCESS

Article

SMC motor proteins extrude DNA asymmetrically and can switch directions

Roman Barth,[1,4] Iain F. Davidson,[2] Jaco van der Torre,[1] Michael Taschner,[3] Stephan Gruber,[3] Jan-Michael Peters,[2] and Cees Dekker[1,5,*]

[1]Department of Bionanoscience, Kavli Institute of Nanoscience Delft, Delft University of Technology, Delft, the Netherlands
[2]Research Institute of Molecular Pathology (IMP), Vienna BioCenter (VBC), Campus-Vienna-Biocenter 1, 1030 Vienna, Austria
[3]Department of Fundamental Microbiology (DMF), Faculty of Biology and Medicine (FBM), University of Lausanne (UNIL), Lausanne, Switzerland
[4]Present address: Institute for Protein Design, Department of Biochemistry, University of Washington, Seattle, WA, USA
[5]Lead contact
*Correspondence: c.dekker@tudelft.nl
https://doi.org/10.1016/j.cell.2024.12.020

SUMMARY

Structural maintenance of chromosomes (SMC) complexes organize the genome via DNA loop extrusion. Although some SMCs were reported to do so symmetrically, reeling DNA from both sides into the extruded DNA loop simultaneously, others perform loop extrusion asymmetrically toward one direction only. The mechanism underlying this variability remains unclear. Here, we examine the directionality of DNA loop extrusion by SMCs using *in vitro* single-molecule experiments. We find that cohesin and SMC5/6 do not reel in DNA from both sides, as reported before, but instead extrude DNA asymmetrically, although the direction can switch over time. Asymmetric DNA loop extrusion thus is the shared mechanism across all eukaryotic SMC complexes. For cohesin, direction switches strongly correlate with the turnover of the subunit NIPBL, during which DNA strand switching may occur. Apart from expanding by extrusion, loops frequently diffuse and shrink. The findings reveal that SMCs, surprisingly, can switch directions.

INTRODUCTION

Genomes across the tree of life are organized and constantly reshaped by active processes within the cell. Structural maintenance of chromosomes (SMC) protein complexes are important, owing to their major role in chromosome organization.[1] The three major members of the SMC family in eukaryotes are condensin, cohesin, and SMC5/6. All three are capable of manipulating DNA via an ATP-dependent process called DNA loop extrusion,[2–10] where loops are created and enlarged stepwise by ATP-binding events to the SMC complex.[9,11] Condensin mainly extrudes DNA loops during mitosis to compact sister chromatids and facilitate chromosome segregation.[12,13] Cohesin organizes interphase chromosomes by looping DNA between convergently oriented CCCTC-binding factor (CTCF) proteins,[14–18] giving rise to topologically associated domains in population-average chromosome-conformation-capture[19–23] as well as imaging experiments,[24–26] which contributes to transcriptional regulation[1,27] as well as genome integrity.[28–30] SMC5/6 has poorly understood functions in chromosome segregation and genome maintenance.[31,32]

The composition and architecture of the three SMC complexes are highly similar (shown schematically for human cohesin in Figure 1A; reviewed previously[33,34]). Two SMC subunits dimerize at their hinge domain and are connected via coiled-coil arms to their heads. The heads harbor ATP-binding domains related to those of ATP-binding cassette (ABC) transporters, which dimerize upon ATP binding to catalyze its hydrolysis. A flexible kleisin subunit bridges the SMC ATPase heads and provides binding sites for two HAWK (HEAT protein associated with a kleisin) proteins in cohesin and condensin or KITE (kleisin-interacting tandem winged-helix element) proteins in SMC5/6.

Despite the overall highly conserved architecture of eukaryotic SMCs and their common ability to extrude DNA loops,[33,35] they appear to significantly differ in their loop extrusion directionality. Here, we use the following terminology to describe the directionality: asymmetric loop extruders incorporate DNA only from one side at a time into the loop, whereas symmetric extruders reel in DNA from both sides simultaneously into the loop. Unidirectional extruders undergo subsequent phases of asymmetric extrusion (possibly interrupted by pauses) that always occur in the same direction, whereas bidirectional extruders exhibit phases of asymmetric extrusion but, here, the side from which DNA is incorporated into the loop switches direction over time (Figures 2A–2D). Yeast condensin is an asymmetric and unidirectional extruder, that is, it reels DNA into the loop strictly from one side,[2,36] whereas human cohesin was reported to reel DNA from both sides into the loop and was thus considered to be a symmetric DNA loop extruder.[3,4] Dimeric yeast SMC5/6 similarly was reported to be a symmetric extruder.[7] Given the

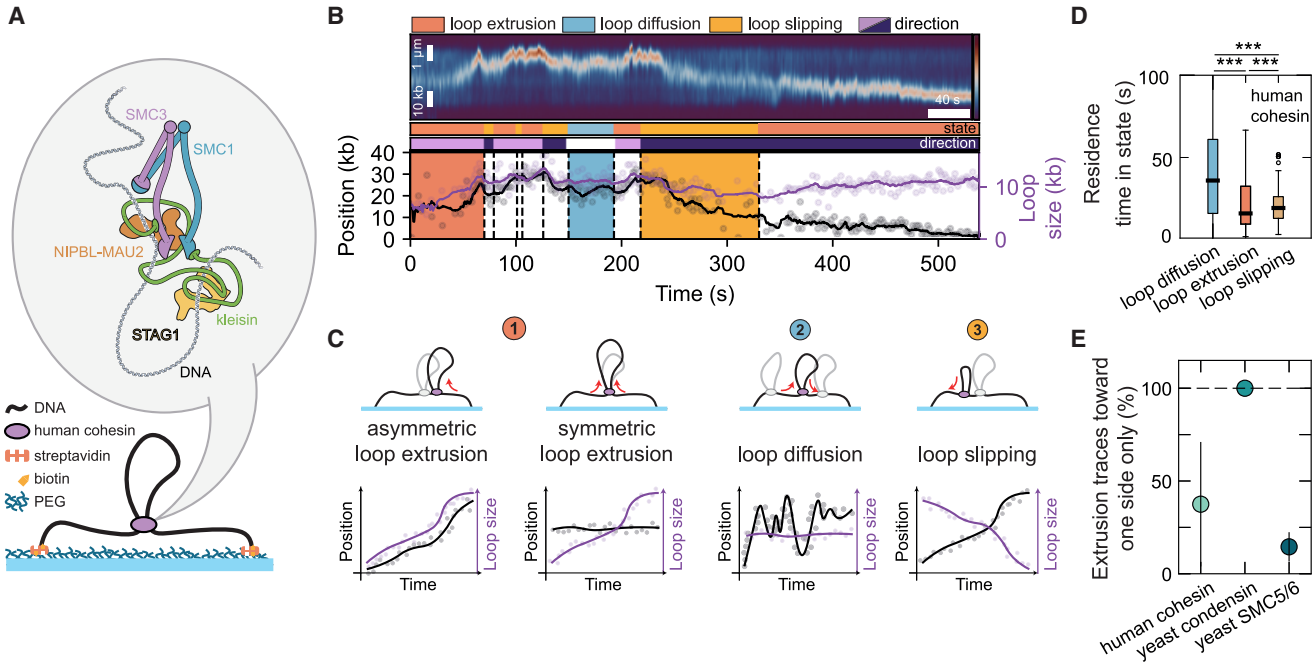

Figure 1. SMC-mediated DNA loop extrusion is interspersed with loop-diffusion and loop-slipping events

(A) Illustration of the DNA loop extrusion assay and the architecture of human cohesin containing SMC3, SMC1, SCC1 (kleisin), NIPBL-MAU2, and STAG1/2 (here only STAG1 is used). The corresponding subunit names for yeast condensin are SMC4, SMC2, BRN1, YCS4, and YCG1. The corresponding subunit names for yeast SMC5/6 are SMC5, SMC6, and NSE4, with additional NSE subunits NSE1, NSE2, and NSE3.

(B) A typical kymograph of cohesin-mediated DNA loop extrusion (NIPBL-MAU2:cohesin ratio 12; 50 mM NaCl). Loop position and size are quantified. Their time propagation permits discerning phases of loop extrusion, diffusion, and slipping. Extrusion and slipping have a direction given by the local sign of the derivative of the loop position with respect to time. Dots represent raw data, solid lines represent a smoothed version using a Savitzky-Golay filter, with window length of 5 s and order 1 (STAR Methods).

(C) Illustration of loop position and size propagation in time for asymmetric and symmetric extrusion, loop diffusion, and slipping.

(D) Duration of diffusion, extrusion, and slipping states (N = 93, 344, and 257, respectively) for human cohesin (pooled from NIPBL-MAU2:cohesin ratios 0.1, 1, 2, and 12; 50 mM NaCl). Black horizontal lines are median values, the box extends between the first and third quartile, and the whiskers extend to 1.5 × IQR (interquartile range). Statistical significance was assessed by a Mann-Whitney test with Bonferroni correction. (*** $p < 0.001$).

(E) Fraction of SMC complexes with at least two extrusion events that displayed only unidirectional extrusion (n = 13, 49, and 29 for cohesin [NIPBL-MAU2:cohesin ratio 2; 50 mM NaCl], condensin, and SMC5/6 [purified from *E. coli*; 100 mM NaCl, 7.5 mM $MgCl_2$], respectively). Error bars denote the binomial 95% confidence interval.

See also Figures S1 and S2.

structural similarity of these complexes,[8,33,34] the reason for these differences is unclear. This variability undermines whether the loop extrusion mechanism[37] is shared among all SMC complexes.

Here, we experimentally measured the directionality of DNA loop extrusion by human cohesin, yeast condensin, and yeast SMC5/6 at a single-molecule level. Close inspection of their loop extrusion dynamics revealed that cohesin and SMC5/6 undergo short phases of active extrusion, characterized by loop growth, which are interspersed by diffusion[3] of the loop and SMC across the DNA, and loop slipping, the gradual loss of the previously extruded loop. Focusing on the extrusion phases, we find that all three monomeric SMC complexes extrude DNA strictly asymmetrically within these phases. Although the condensin holocomplex is a strictly unidirectional extruder, cohesin and monomeric SMC5/6 undergo frequent direction switches, making them bidirectional loop extruders. Furthermore, we found that human cohesin undergoes direction switches upon exchange of its HEAT subunit NIPBL (Nipped-B-like protein). These findings indicate that the DNA loop extrusion mechanism is inherently asymmetric and is likely common to all SMC complexes.

RESULTS

Phases of active DNA loop extrusion are interspersed by loop diffusion and loop slipping

To characterize the dynamics of DNA loop extrusion by human cohesin in detail, we reconstituted DNA loop extrusion with purified proteins at the single-molecule level *in vitro*. To this end, λ-DNA, which served as a substrate for loop extrusion, was tethered at both ends onto a polyethylene glycol-passivated glass surface at an extension of ∼30% of its contour length. DNA was visualized using SYTOX Orange intercalating dye and imaged using highly inclined and laminated optical sheet (HILO) microscopy (STAR Methods). Human cohesin, NIPBL-MAU2, and ATP were subsequently introduced into the flow

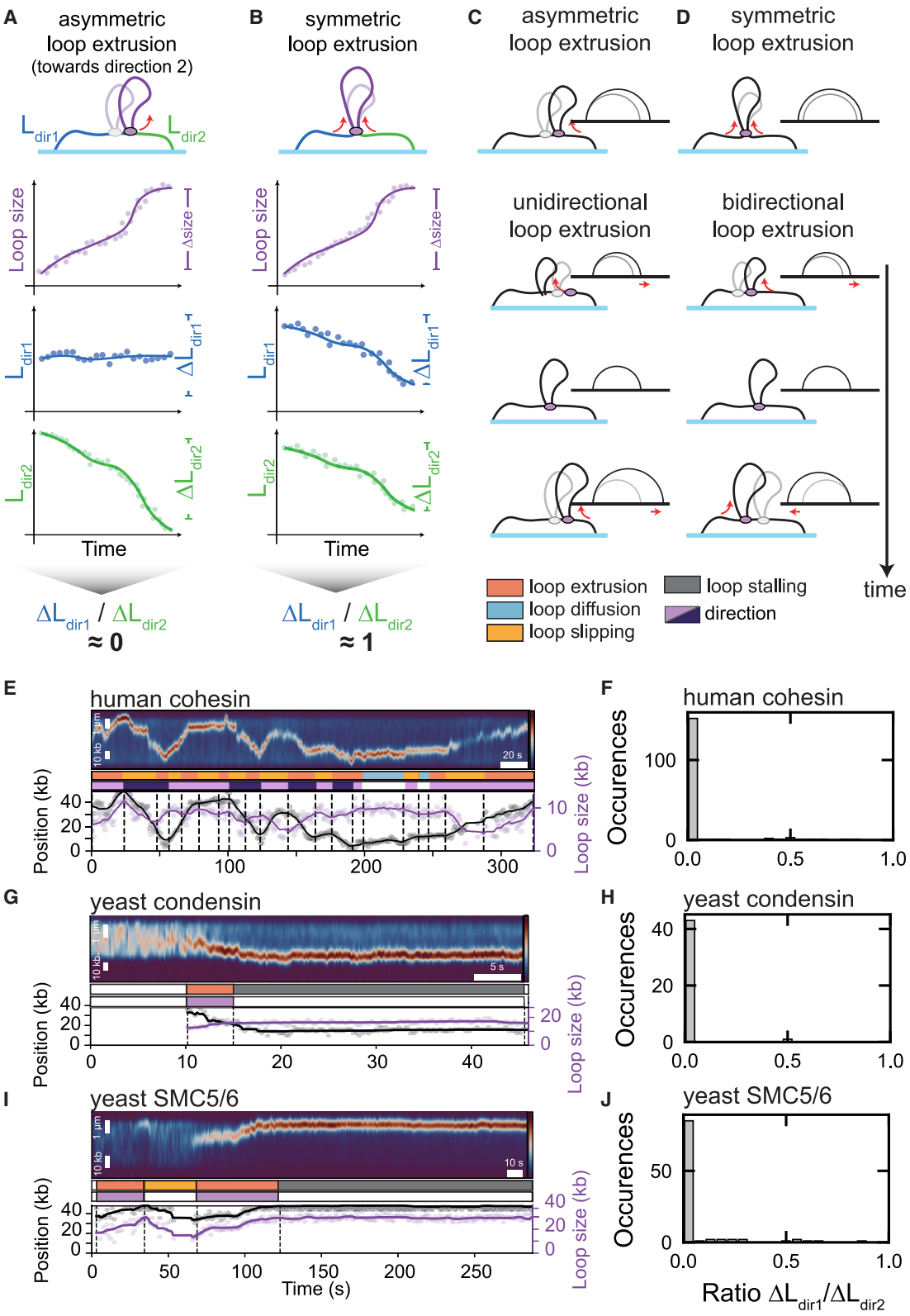

(legend on next page)

channel and the flow was stopped to record cohesin-mediated loop extrusion in the absence of buffer flow (Figure 1A). Kymographs were constructed that served as the basis for quantifying the size of the loop and its position (Figure 1B; STAR Methods).

The time propagation of these two independent quantities, loop size and position, defines distinct phases into which loop extrusion traces were segmented (STAR Methods; Figures 1C and S1A): (1) phases of active DNA loop extrusion exhibited an increase in loop size (Figures 1C and red shading in 1B); (2) extended "loop diffusion" periods in which the loop size remained approximately constant, while the loop position changed in a diffusive manner (Figures 1C, blue shading in 1B, and S1I), as noted previously[3]; and (3) gradual shrinking of loops (Figures 1B, yellow shading in 1C, and S1J), as noted previously as a possible outcome of cohesin-CTCF encounters.[15] Phases of loop stalling, e.g., by reaching the end of surface-tethered DNA molecules, were excluded (e.g., Figure 2). This gradual shrinkage is distinct from a sudden step-wise loop rupture, which resolves the loop within one or a few frames (~100 ms).[2,36] Loop shrinkage typically only led to a partial (i.e., incomplete) loss (Figures S1C, S1D, and S1J). Quantitatively, cohesin remained longest in the diffusive state (41 ± 44 s, median ± SD), although spending 16 ± 17 s (median ± SD) in active extrusion, which was comparable with the time spent in the loop slipping phases (20 ± 15 s, median ± SD; Figure 1D). We tested whether even shorter phases existed, which could have been missed by acquiring images at a frame rate of 5–10 frames per second (fps). Acquired images at 50 fps yielded no significantly shorter phases however (STAR Methods; Figures S1E–S1H).

To examine how the loop extrusion dynamics among the three eukaryotic SMC complexes differed, we repeated the experiments and analyses with budding yeast condensin and budding yeast SMC5/6 (STAR Methods; Figure S2). First, we tested whether the purified SMC5/6 used here is able to perform DNA loop extrusion, as reported previously[7] (Figure S2). Indeed, we confirmed that SMC5/6 exhibits loop extrusion of DNA with similar characteristics as reported (Figures S2B–S2E), although we found that yeast SMC5/6—like human cohesin and yeast condensin—already extrudes as a monomer (Figures S2F–S2J), whereas Pradhan et al.[7] reported loop extrusion only for SMC5/6 dimers. This held true both for SMC5/6 expressed and purified from *E. coli* (Taschner and Gruber[38]) as well as from *S. cerevisiae* (Pradhan et al.[7]; compare Figures S2G and S2I). For experiments in a low-salt buffer (50 mM NaCl, 2.5 mM $MgCl_2$) with SMC5/6 expressed and purified from *E. coli*, we observed a smaller fraction of SMC5/6 complexes undergoing bidirectional extrusion compared with experiments performed in a buffer containing 100 mM NaCl and 7.5 mM $MgCl_2$ (for purifications both from *E. coli* and yeast). Due to the finite labeling efficiency, we cannot exclude the possibility that the fraction of bidirectionally extruding SMC5/6 complexes purified from *E. coli* in the low-salt buffer were dimeric SMC5/6. However, bidirectional extrusion by SMC5/6 in the high-salt buffer is unlikely (at 0.1% and 5% significance level for purifications from *E. coli* and yeast, respectively) to be the result of SMC5/6 dimers because the fraction of potential SMC5/6 dimers in these conditions is significantly lower than the fraction of bidirectionally extruding SMC5/6 complexes (Figure S2K; STAR Methods). Although SMC5/6 exhibited dynamics comparable with cohesin, condensin exhibited only brief phases of diffusion (7 ± 4 s, median ± SD), whereas extrusion phases lasted 13 ± 9 s (median ± SD) and loop slipping was hardly ever observed (1/65 phases; Figure S1M).

All eukaryotic SMC complexes extrude DNA asymmetrically

The growth and concomitant change in the loop position is a proxy for the direction of DNA loop extrusion, as illustrated in Figure 1C. By monitoring the direction of travel of the loop extrusion phases during the experiment (from the start of the extrusion until loop dissolution or the end of acquisition), we measured the fraction of SMC complexes that showed multiple extrusion phases in the same or opposite directions. Although condensin is a strictly unidirectional extruder (all extrusion phases moved toward one side of the DNA), 40%–60% of cohesin and ~80% of SMC5/6 complexes that show at least two extrusion phases extruded toward both sides during the course of the experiment (Figures 1B, 1E, and S1D).

Cohesin-mediated loop extrusion phases were mostly interspersed with either a diffusion or a slipping phase (or both) between subsequent extrusion phases (Figure S1K); switches between extrusion and slipping phases were most common

Figure 2. All eukaryotic SMC complexes extrude DNA in an asymmetric manner

(A) Illustration of loop size and amount of DNA left and right of the loop in time for asymmetric loop extrusion.

(B) Illustration of loop size and amount of DNA left and right of the loop in time for symmetric loop extrusion. The ratio of changes in amount of DNA left and right of the loop is discriminative between asymmetric and symmetric extrusion.

(C) Unidirectionally extruding SMC complexes undergo one or multiple phases of asymmetric active loop extrusion in the same direction throughout their loop lifetime.

(D) During symmetric DNA loop extrusion, DNA is reeled in from both sides into the loop. In contrast, bidirectionally extruding SMC complexes undergo subsequent phases of asymmetric extrusion with changing directions.

(E) Example loop extrusion kymograph of cohesin (NIPBL-MAU2:cohesin ratio 7; 50 mM NaCl) with loop position and size quantification and segmentation into phases of extrusion, diffusion, and slipping. Dots represent raw data, solid lines represent a smoothed version using a Savitzky-Golay filter with window length of 5 s and order 1 (STAR Methods).

(F) Distribution of the ratio $\Delta L_{dir1}/\Delta L_{dir2}$ for extrusion events of human cohesin (n = 166 events; pooled from NIPBL-MAU2:cohesin ratios 0.1, 1, 2, and 12; 50 mM NaCl).

(G) Example kymograph of unidirectional DNA loop extrusion for yeast condensin as in (E).

(H) Distribution of the ratio $\Delta L_{dir1}/\Delta L_{dir2}$ distribution for yeast condensin (n = 44 events).

(I) Example kymograph of unidirectional DNA loop extrusion for yeast SMC5/6 (purification from *E. coli*; 50 mM NaCl, 2.5 mM $MgCl_2$) as in (E).

(J) Distribution of the ratio $\Delta L_{dir1}/\Delta L_{dir2}$ distribution for yeast SMC5/6 (N = 100 events; purification from *E. coli*; 100 mM NaCl, 7.5 mM $MgCl_2$).

See also Figures S1 and S2.

(Figure S1L). Direction switches without intervening diffusion or slipping phases were less common, as only approximately 25% of direction switches occur during loop extrusion, i.e., without observable intermittent diffusion or slipping phase (Figure S1K). The sequence of extrusion, diffusion, and slipping phases can be described as a first-order Markov chain; that is, the transition probabilities between the states solely depend on the current state, indicating that the system is memory-less (Figure S3D).

Asymmetric and symmetric DNA loop extruders are characterized by their ability to reel DNA into the loop from one or both sides, respectively.[2,7] For an asymmetric extruder, the stretch of DNA on one side of the SMC becomes progressively shorter, while the length of the other side remains constant[2] (Figure 2A). In contrast, both arms become simultaneously shorter as the loop is being enlarged by a symmetric extruder (Figure 2B). Thus, the ratio of the length changes on both sides of the loop during loop extrusion constitutes a quantity that we name a "symmetry indicator," which is close to 0 for an asymmetric extruder (because $\Delta L_{dir1} \approx 0$ in Figure 2A) and ≈ 1 for a symmetric extruder. Note that the definitions of (a)symmetric loop extrusion are distinct from uni-/bidirectional extrusion (Figures 2C and 2D). Uni- and bidirectional extruders both undergo subsequent phases of asymmetric extrusion. However, unidirectional extruders always extrude DNA from the same side into the loop (e.g., yeast condensin[2,36]), whereas bidirectional extruders exchange the side from which DNA is reeled into the loop in between subsequent extrusion phases (and rarely without intermittent loop diffusion/slipping phase; Figure S1K). Therefore, symmetric extruders are always bidirectional extruders, whereas asymmetric extruders can extrude bi- or unidirectionally, depending on whether they switch their direction of extrusion or not.

To determine whether cohesin extrudes DNA asymmetrically or symmetrically, we computed the symmetry indicator $\Delta L_{dir1}/\Delta L_{dir2}$ within the duration of the segmented loop extrusion phases (the durations are shown in Figures 1D and S1M). We found that 92% ± 4% (mean ± 95% binomial confidence interval, n = 166) of all extrusion phases exhibited a value of $\Delta L_{dir1}/\Delta L_{dir2}$ below 0.1 (Figure 2F). Extrusion phases of yeast condensin, a known asymmetric extruder[2] (Figure 2G), used here as a positive control, exhibited a similar distribution, with 98% ± 4% (mean ± 95% binomial confidence interval, n = 44, Figure 2H) of all values of $\Delta L_{dir1}/\Delta L_{dir2}$ below 0.1. Yeast SMC5/6 (Figure 2I) also exhibited asymmetric extrusion phases (86% ± 7% [mean ± 95% binomial confidence interval] of $\Delta L_{dir1}/\Delta L_{dir2}$ values below 0.1, n = 100, Figures 2J and S3A). Notably, the slipping phases of cohesin and SMC5/6 were also asymmetric (Figures S3B and S3C), suggesting that loop slipping is the result of weak DNA binding at either the motor or anchor side of the SMC complexes but not both. In contrast, we expect that loop diffusion is the result of weakened (but non-zero) DNA binding at the motor or anchor side of SMC complexes.

We conclude that all eukaryotic SMC complexes extrude DNA asymmetrically, strictly toward one direction at a time; however, cohesin and SMC5/6 may switch the direction of extrusion between two successive extrusion phases.

NIPBL excess increases the chance to observe direction switches

Even though yeast condensin is a strictly unidirectional DNA loop extruder, the complex extrudes in both directions, alternating when YCG1, condensin's "anchor" (Shaltiel et al.[36]), is deleted or when the strong DNA-binding site within the safety belt[39] is mutated. These results suggest that weakening or dissolution of at least one DNA-binding site is required to permit direction switches during DNA loop extrusion. Human cohesin requires a reservoir of unbound NIPBL-MAU2 for ongoing DNA loop extrusion and loop maintenance,[3] and *in vivo* fluorescence recovery after photobleaching (FRAP) experiments indicated that NIPBL-MAU2 hops from cohesin to cohesin in cells,[40] suggesting that NIPBL-MAU2 is only transiently bound to cohesin as NIPBL-MAU2 heterodimers continuously exchange on cohesin. As NIPBL-MAU2 contains a strong DNA-binding site,[41] we hypothesized that dissociation of NIPBL-MAU2 from the complex weakens the DNA-binding site close to the SMC3 subunit, which could subsequently lead to extrusion direction switches.

To test this, we performed cohesin-mediated DNA loop extrusion experiments with varying concentrations of NIPBL-MAU2 to modulate the average occupancy of NIPBL-MAU2 on cohesin. In loop extrusion experiments where NIPBL-MAU2 was added at a sub-stoichiometric ratio to cohesin, mostly unidirectional extrusion was observed (Figures 3A, ratio of NIPBL-MAU2 to cohesin = 0.1 and 3D). Strikingly, upon increasing the NIPBL-MAU2:cohesin ratio, more traces with extrusion phases toward both directions were observed (Figures 3A and 3E–3G). In addition, the fraction of cohesin complexes that underwent diffusion and loop slipping increased with increasing NIPBL-MAU2:cohesin concentration ratios (Figures S3E and S3F). Bidirectional extrusion cannot be attributed to the dimerization of cohesin, as suggested previously,[4] because in both uni- and bidirectional extrusions, mostly a single cohesin complex colocalized with the loop[3] (Figures S3G, S3H, and S3J). In response to increasing the NIPBL-MAU2:cohesin ratio, bidirectional DNA loop extrusion by cohesin was more often observed before the loop vanished. However, we did not find an enhanced direction switching frequency (Figure 3B), or a changing time between subsequent extrusion phases (Figure S4E), or an enhanced frequency of entering a diffusion or slipping phase (Figures S4C and S4D) in response to a higher NIPBL-MAU2:cohesin ratio. Instead, the loop lifetime, the time between the beginning of the first extrusion phase until loop dissolution, increased as a larger excess of NIPBL-MAU2 over cohesin was supplied (Figures 3C and S4F), in line with previous loop maintenance assays,[3] giving cohesin more time to switch extrusion direction or enter diffusion and slipping phases before the loop vanishes. Subsequent extrusion phases were indistinguishable in terms of the loop extrusion rate (Figure S3I). These results suggest that the rebinding of NIPBL to cohesin stabilizes loops and that cohesin can undergo additional loop extrusion cycles in any direction upon rebinding of a NIPBL molecule.

In the absence of NIPBL, loops can diffuse and slip but cannot be extruded

Next, we aimed to directly visualize whether an exchange of NIPBL-MAU2 on cohesin occurs. Because NIPBL-MAU2

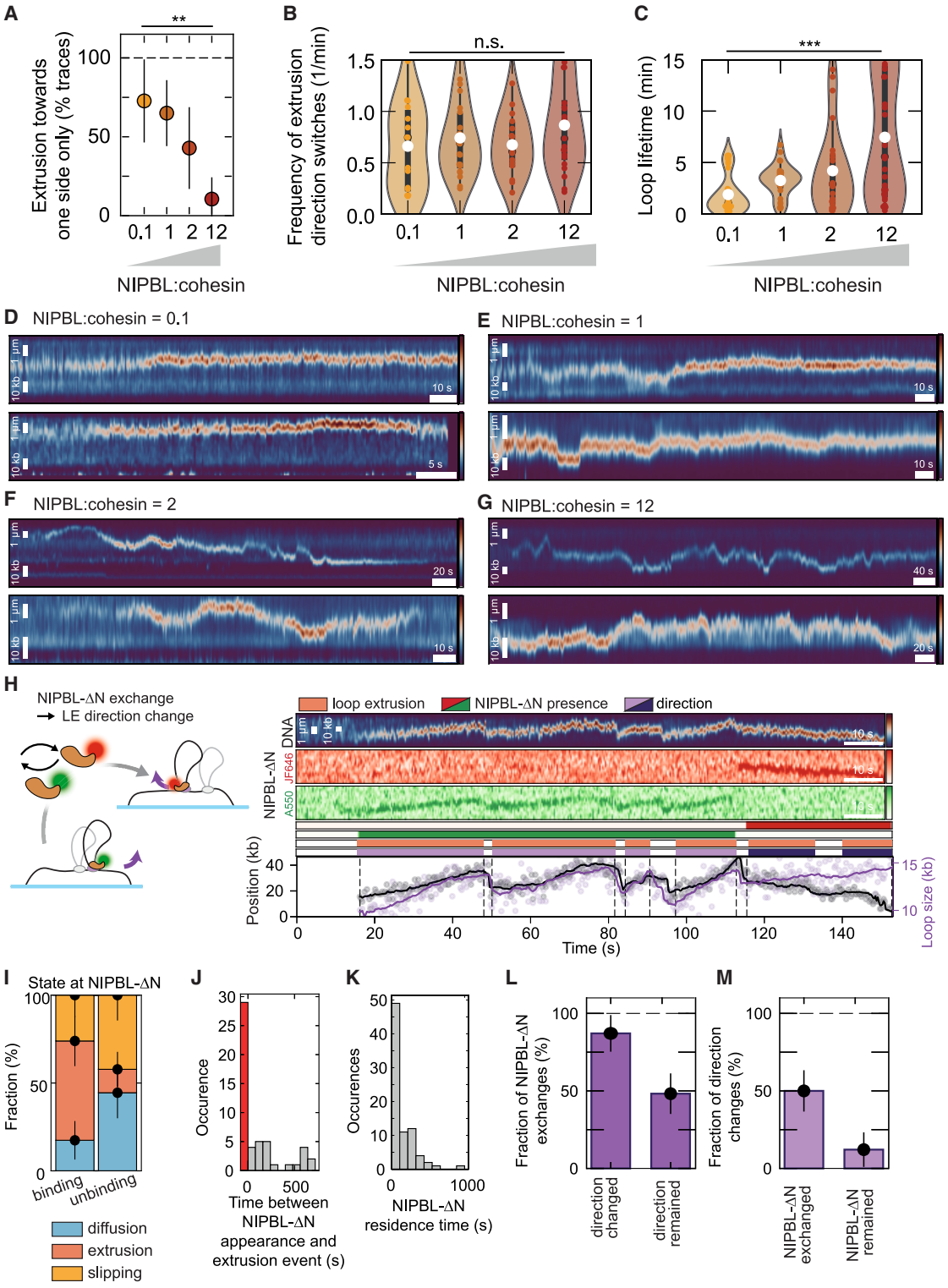

Figure 3. DNA loop extrusion direction switches coincide with an exchange of NIPBL-ΔN

(A) Fraction of cohesin complexes undergoing at least two extrusion events that displayed only unidirectional extrusion for varying ratios of NIPBL-MAU2:cohesin at 50 mM NaCl (n = 41, 30, 17, and 26 from left to right). Error bars denote the binomial 95% confidence interval. Statistical significance was assessed by a chi-squared test (**p = 0.0013).

(legend continued on next page)

displays a propensity to accumulate/aggregate,[3] we expressed and purified an N-terminal truncation of NIPBL (NIPBL-ΔN; Bauer et al.[41]), alleviating this limitation. Experiments with NIPBL-ΔN were carried out in a buffer containing 25 mM NaCl, which boosted the frequency of loops with NIPBL-ΔN and helped to improve binding of SYTOX Green to DNA and thus visualization of DNA (for NIPBL-ΔN-A550 imaging, see below) compared with a buffer containing 50 mM NaCl. These changes in ionic strength and swapping between NIPBL-MAU2 and NIPBL-ΔN did not affect DNA loop extrusion dynamics by cohesin (Figure S4). NIPBL-ΔN was split into two batches that were labeled differentially with ATTO 550 (NIPBL-ΔN-A550) and Janelia Fluor 646 (NIPBL-ΔN-JF646) fluorophores (STAR Methods; Figure S5A). We then performed cohesin-mediated DNA loop extrusion experiments with an equimolar ratio of NIPBL-ΔN-A550 and NIPBL-ΔN-JF646 and monitored the presence and absence of NIPBL-ΔN in the two colors colocalizing with the loop (Figures 3H and S5B–S5E). Loops did not grow further in the absence of NIPBL-ΔN, suggesting that cohesin cannot actively extrude DNA in the absence of NIPBL. NIPBL-ΔN binding to loops (likely bound to the cohesin complex that previously extruded the loop) typically coincided with the start of a loop-extrusion phase, but NIPBL-ΔN also bound to cohesin during diffusion and slipping phases (Figure 3I, left bar). In the latter case, the next extrusion phase followed within a few minutes (142 ± 222 s [mean ± SD], Figure 3J). Dissociation of NIPBL-ΔN occurred most often during diffusion or slipping phases, on average 31 ± 53 s (mean ± SD) after the last extrusion phase (Figure S5F) and only rarely at the end of extrusion phases (Figure 3I, right bar), after NIPBL-ΔN spent on average 161 ± 186 s (mean ± SD) bound to the loop (likely bound to the cohesin that previously extruded the loop; Figure 3K). An extruded loop without bound NIPBL-ΔN at its base was typically rebound by NIPBL-ΔN after ∼1–2 min (Figure S5G) though loops without bound NIPBL-ΔN were observed for up to 5 min (at NIPBL-ΔN:cohesin ratio of 0.1–1 in these experiments), which is in agreement with the report that, in the absence of NIPBL-MAU2, most loops dissociated within 8 min (Davidson et al.[3]). The diffusion constant of diffusing loops as well as the loop slipping rate were not significantly different in the presence or absence of NIPBL-ΔN (Figures S5H and S5I), suggesting that NIPBL does not contribute to DNA binding during the diffusion and slipping phases. Because NIPBL is known to contribute to DNA clamping onto the ATPase heads upon ATP binding,[42,43] this suggests that the diffusion and slipping phases represent ATP-unbound states of cohesin. Imaging and bleaching of labeled NIPBL-ΔN excluded the possibility that the increased loop lifetime is a result of protein accumulation at loops because we observed a similar distribution of bleaching steps (mostly 1 step) irrespective of the ratio of NIPBL-ΔN to cohesin (Figures S3K, S3L and S4).

Extrusion direction switches coincide with an exchange of NIPBL on cohesin

Next, we analyzed how an exchange of NIPBL-ΔN relates to the extrusion direction switching of cohesin. We considered an exchange of NIPBL-ΔN if the fluorescence intensity of one label was replaced with an intensity of the other label, as well as when the fluorescence intensity of one label disappeared and re-appeared at least 2 frames later. Note that imposing this restriction allowed us to monitor exchanges between NIPBL-ΔN carrying the same label only as long as the loop-extruding cohesin remained unbound by NIPBL-ΔN for at least 600 ms. Figure 3H shows an example kymograph of cohesin-mediated loop extrusion in which, first, (15–112 s) four successive extrusion phases move toward the upper end of the DNA molecule with intermittent

(B) Frequency of extrusion direction switches for varying ratios of NIPBL-MAU2:cohesin at 50 mM NaCl (n = 41, 30, 17, and 26). The white dot denotes the mean. The box shows the quartiles of the dataset and the whiskers extend to 1.5 × IQR. Statistical significance was assessed by a Kruskal-Wallis test (n.s. p = 0.19).
(C) Loop lifetime between the first extrusion event and loop disruption for varying ratios of NIPBL-MAU2:cohesin at 50 mM NaCl (N = 41, 31, 25, and 37). The white dot denotes the mean. The box shows the quartiles of the dataset and the whiskers extend to 1.5 × IQR. Statistical significance was assessed by a Kruskal-Wallis test (***$p < 0.001$).
(D) Example kymographs of cohesin-mediated loop extrusion at NIPBL-MAU2:cohesin = 0.1 at 50 mM NaCl. Dots represent raw data, solid lines represent a smoothed version using a Savitzky-Golay filter with window length of 5 s and order 1 (STAR Methods).
(E) Example kymographs of cohesin-mediated loop extrusion at NIPBL-MAU2:cohesin = 1 at 50 mM NaCl as in (D).
(F) Example kymographs of cohesin-mediated loop extrusion at NIPBL-MAU2:cohesin = 2 at 50 mM NaCl as in (D).
(G) Example kymographs of cohesin-mediated loop extrusion at NIPBL-MAU2:cohesin = 12 at 50 mM NaCl as in (D).
(H) Example trace where the exchange of NIPBL-ΔN coincides with a switch in the loop extrusion direction. Cohesin extrudes toward the lower end as long as the ATTO 550-labeled NIPBL-ΔN is bound to cohesin. After exchange to a JF646-labeled NIPBL-ΔN, cohesin extrudes toward the upper end. HeLa cohesin was used with NIPBL-ΔN-ATTO550 and NIPBL-ΔN-JF646 at NIPBL-ΔN:cohesin ratio 0.1 in 25 mM NaCl. Dots represent raw data, solid lines represent a smoothed version using a Savitzky-Golay filter with window length of 5 s and order 1 (STAR Methods).
(I) Probability of states at which NIPBL-ΔN binds to cohesin (n = 46) and at which NIPBL-ΔN dissociates (n = 45). Binding and unbinding at extrusion phases was only observed concomitant with the start/end of extrusion phases, respectively (NIPBL-ΔN:cohesin ratio 0.1 in 25 mM NaCl). The bar height indicates the probability of a given state and the error bar denotes the binomial 95% confidence interval.
(J) Distribution of time between NIPBL-ΔN appearance and the next extrusion event (n = 56; NIPBL-ΔN:cohesin ratio 0.1 in 25 mM NaCl). The red bar represents the occurrences when NIPBL-ΔN appearance coincided with the start of an extrusion event.
(K) Distribution of NIPBL-ΔN residence times (n = 47; NIPBL-ΔN:cohesin ratio 0.1 in 25 mM NaCl).
(L) Fraction of cohesin molecules for which NIPBL-ΔN exchanged in between direction switches (87% ± 12%, n = 31) and the fraction of cohesin molecules on which NIPBL-ΔN exchanged without direction switch between successive extrusion phases (48% ± 13%, n = 56) at NIPBL-ΔN:cohesin ratio 0.1 in 25 mM NaCl. Error bars denote the binomial 95% confidence interval.
(M) Fraction of direction switches between successive extrusion phases during which NIPBL-ΔN exchanged (50% ± 13%, n = 54) and the fraction of direction switches between successive extrusion phases during which NIPBL-ΔN remained (12% ± 11%, n = 33) at NIPBL-ΔN:cohesin ratio 0.1 in 25 mM NaCl. Error bars denote the binomial 95% confidence interval.
See also Figures S3–S5.

loop slipping phases. During all these unidirectional phases, a NIPBL-ΔN-A550 molecule colocalized with the DNA loop (presumably bound to cohesin[3]), which, however, dissociated from the loop/cohesin at t = 113 s. At t = 116 s, a NIPBL-ΔN-JF646 bound to the loop/cohesin, which coincided with a direction switch as extrusion of the loop now proceeded toward the lower end of the DNA molecule. We monitored such an appearance and disappearance of NIPBL-ΔN in relation to direction switches for multiple molecules (additional examples in Figures S5B–S5E). In 86% ± 12% of the cases in which a direction switch was observed, there was also an exchange of NIPBL-ΔN between extrusion phases in opposite directions (e.g., Figure S5B). When subsequent extrusion phases occurred in the same direction, an exchange of NIPBL-ΔN was observed in 52% ± 12% of the cases (Figure 3L, example in Figure S5D). Conversely, an exchange of NIPBL-ΔN coincided in 47% ± 12% of the cases with a direction switch, whereas only 14% ± 11% of the cases in which a direction switch was observed did not correlate with an exchange of NIPBL-ΔN (Figure 3M).

These data show that extrusion direction switches coincide with an exchange of NIPBL, strongly suggesting that NIPBL exchange is a necessary step to permit extrusion direction switches. The opposite is, however, not true: an exchange of NIPBL does not necessarily yield a direction switch. It is possible that NIPBL molecules carrying the same fluorophore did exchange within a time period that could not be resolved (using the time resolution of 300 ms used in these experiments). Events in which direction switches were observed without concomitant NIPBL exchange might have been caused by such events (Figures 3L, first bar and 3M, second bar). Alternatively, it is possible that NIPBL exchange is not strictly required to switch extrusion directions because Shaltiel et al. observed direction switches of yeast condensin in the absence of YCG1 without an apparent exchange of YCS4 (Shaltiel et al.[36]). Instead, temporary unbinding of NIPBL from DNA may be sufficient to allow direction switches (discussed below). In conclusion, the rate of the NIPBL dissociation from cohesin determines the rate of direction switching (which is thus independent of the NIPBL:cohesin ratio; Figure 3B). In contrast, the loop lifetime is limited by a NIPBL molecule binding to cohesin and thus depends on the NIPBL:cohesin ratio (Figure 3C).

Extrusion direction switching, loop diffusion, and loop slipping explain features of interphase chromosome organization

Previous 3D polymer simulations have shown that a model in which DNA loop extruders switch their direction of extrusion over time recapitulates the interphase chromosome organization, as observed by Hi-C or related techniques, better than a model in which SMCs extrude DNA unidirectionally.[44] Here, we replicate and extend these simulations to assess the effect of loop diffusion and slipping phases (as observed *in vitro*, e.g., Figure 1) on chromosome contact maps. To this end, we combinatorically add bidirectional (i.e., switching, in contrast to unidirectional) and/or diffusing and slipping loop extruders to stochastic simulations of loop-extrusion dynamics before sampling the 3D polymer dynamics (STAR Methods). If allowed, extruders switch stochastically with a rate as measured *in vitro* (Figure 3B). If loop diffusion and slipping are allowed, loops spawn in an extrusion state and switch to a diffusion state, with a probability of 80%, or a slipping state, with a probability 20% (Figure S1L). The switching rate from any state to the next is given by the average duration of the current phase (Figure 1D; STAR Methods).

Purely unidirectionally extruding SMCs produce "stripes" at boundary elements but fail to produce loops between boundary elements ("corner dots"), as noted previously.[44] This occurs because extruders attempt only once to pass a boundary element and get stuck there until dissociation of the extruder. Extruders thus only encounter one boundary element, but never both (unless the extruder spawns at a boundary element), generating stripes at boundary elements. When unidirectional extruders are allowed to undergo diffusion and slipping phases, stripes become fainter and extended stripes become faintly apparent. Boundary-element-stalled extruders undergoing diffusion may repeatedly attempt to cross a boundary element due to repeated extrusion and slipping in the same direction, as well as diffusion in the vicinity of a boundary element. This increases the chance of an extruder to eventually overcome the boundary element, generating contacts and stripes beyond the first boundary element. Note, however, that the features are weak and no primary dots are observed.

When extruders are allowed to switch (without diffusion and slipping), both stripes and corner dots are observed, as well as the onset of extended stripes and dots. In this scenario, extruders encounter one boundary element and likely get stalled. After some time, the extrusion direction switches and the extruder can reel in DNA until the second boundary element is encountered, generating corner dots. Repeated attempts to overcome a boundary due to direction switching also generates extended corner dots and stripes. When diffusion and slipping phases are added to switching extruders, the resulting contact map shows corner dots and stripes to a slightly weaker extent than to purely bidirectionally extruding SMCs. However, because extruders can, in addition to extruding, also diffuse and slip in either direction, SMCs have a higher chance to overcome boundary elements and thus generate larger loops and more extended stripes and dots. The resulting contact maps resembles the experimental Hi-C contact maps more closely in terms of extended dots and stripes and their strength (Figure 4B). We conclude that switching of loop extruders, but also loop diffusion and slipping of extruded loops, explains features of the interphase chromosome organization *in vivo*.

DISCUSSION

DNA loop extrusion is conserved, asymmetric, and can switch direction

DNA loop extrusion is an important molecular mechanism across the tree of life. Although yeast condensin has been reported to extrude DNA from one side only,[2] human cohesin[3,4] and yeast SMC5/6 (Pradhan et al.[7]) were found to reel in DNA from both sides, suggesting that cohesin and SMC5/6 are symmetric extruders. These differential loop extrusion dynamics questioned whether the DNA loop extrusion mechanism is conserved among eukaryotic SMC complexes. Using single-molecule *in vitro* reconstitution of DNA loop extrusion by all three eukaryotic

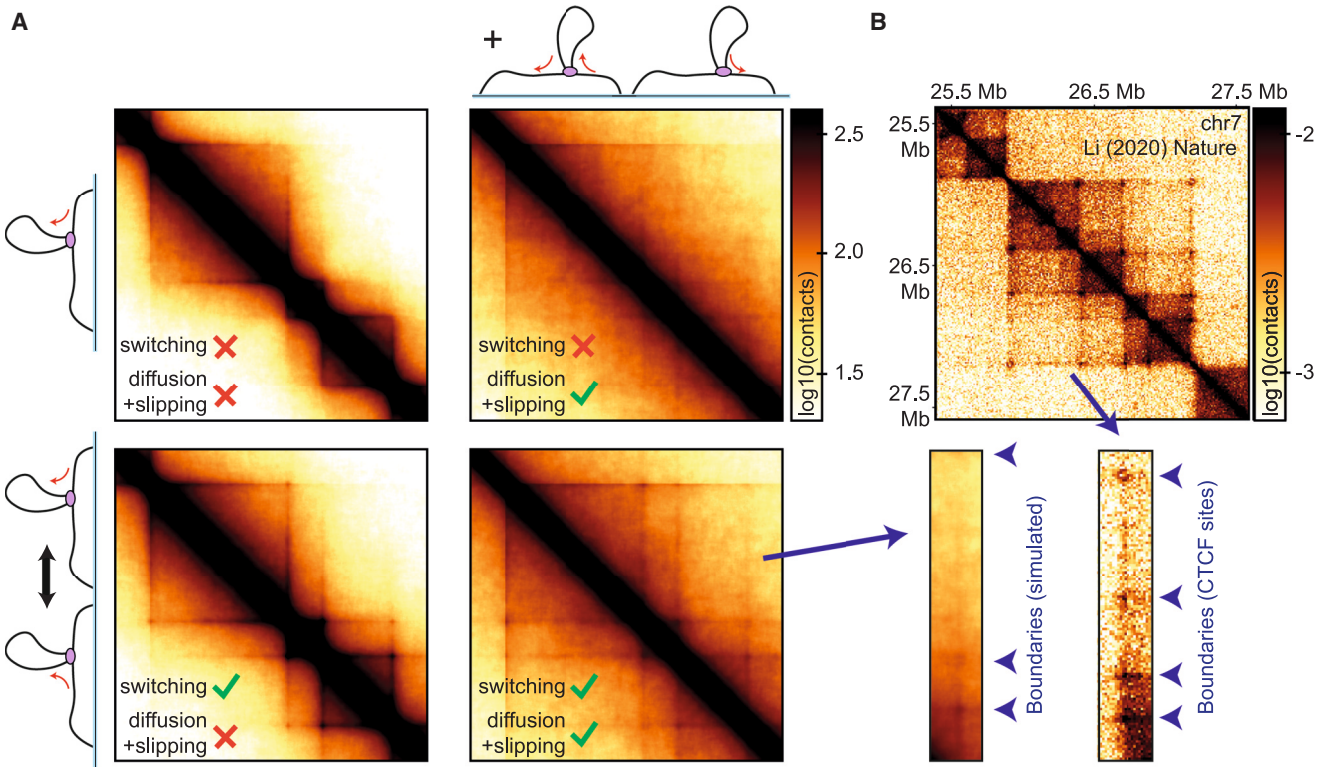

Figure 4. 3D polymer simulations of a model interphase chromosome extruded by SMC complexes undergoing direction switching, loop diffusion, and switching

(A) Contact maps computed from polymer simulations in which loop extruders do or do not undergo direction switching, loop diffusion, and loop slipping at a resolution of 2 kb.

(B) Hi-C contact matrix of the HOXA locus (hg19, 10 kb resolution[17]), visualized by HiGlass (data from Kerpedjiev et al.[45]).

SMCs and quantification of their loop extrusion dynamics, we set out to clarify whether an asymmetric DNA loop extrusion mechanism may constitute the common *modus operandi* of the eukaryotic SMCs. Indeed, we found that all monomeric eukaryotic SMCs extrude DNA strictly asymmetrically (Figure 2). However, cohesin and SMC5/6 are able to switch the direction of extrusion (Figure 1E). These results strongly suggest that the DNA loop extrusion mechanism is shared among the eukaryotic SMCs (potentially including the prokaryotic SMCs as well), is inherently asymmetric, and that the DNA loop extrusion cycle permits direction switches.

Our results suggest that direction switches require an exchange of NIPBL on human cohesin (Figure 3). The propensity of cohesin and condensin to switch extrusion directions can likely be tuned by modulating the ability to bind DNA at either the HEAT-A subunit (NIPBL/YCS4, respectively), HEAT-B subunit (STAG1/YCG1), or both. For cohesin, dissociation of NIPBL likely weakens a DNA-binding site close to SMC3 (the motor side) because NIPBL forms a strong DNA-binding site on the cohesin holocomplex.[41] Note that the dissociation and rebinding of DNA-binding subunits is an extreme measure to temporarily weaken DNA binding at these subunits. In order to allow direction switches via DNA strand exchange (see below), DNA is only required to temporarily unbind from the motor (NIPBL/YCS4 or equivalent) and anchor (STAG1/STAG2/YCG1), while both HEAT subunits could remain bound to cohesin and condensin, respectively. The fact that direction switches are observed for ΔYCG1 condensin, even though YCS4 was intact in these experiments,[36] suggests that DNA can indeed temporarily unbind from YCS4 (and potentially other HEAT and KITE subunits) without complete subunit dissociation from the complex.

This might also explain why both uni- and bidirectional extrusion has been observed concomitantly for human condensin I and II (Kong et al.[10]) and for *X. laevis* condensin from egg extracts,[5] where no subunit turnover is known. The loop extrusion activity of human cohesin, but not of condensin, is regulated *in vivo* by the replacement of NIPBL by Pds5/WAPL.[3,18,46–50] This might explain why NIPBL dynamically exchanges on cohesin, whereas analogous subunits do not for other SMC proteins.

Mechanistic models that enable DNA strand exchange

How can a DNA-loop-extrusion model account for direction switches? We envision two possible scenarios that extend the recently proposed reel-and-seal model,[37] based on previous considerations in which DNA strands between the motor and anchor sides are exchanged ("DNA strand exchange") to enable extrusion direction switches,[6,36] see Figures 5 and S6. The stem of the DNA loop is bound to at least two DNA-binding sites: the motor subunit (NIPBL) and the anchor subunit (STAG1/2).

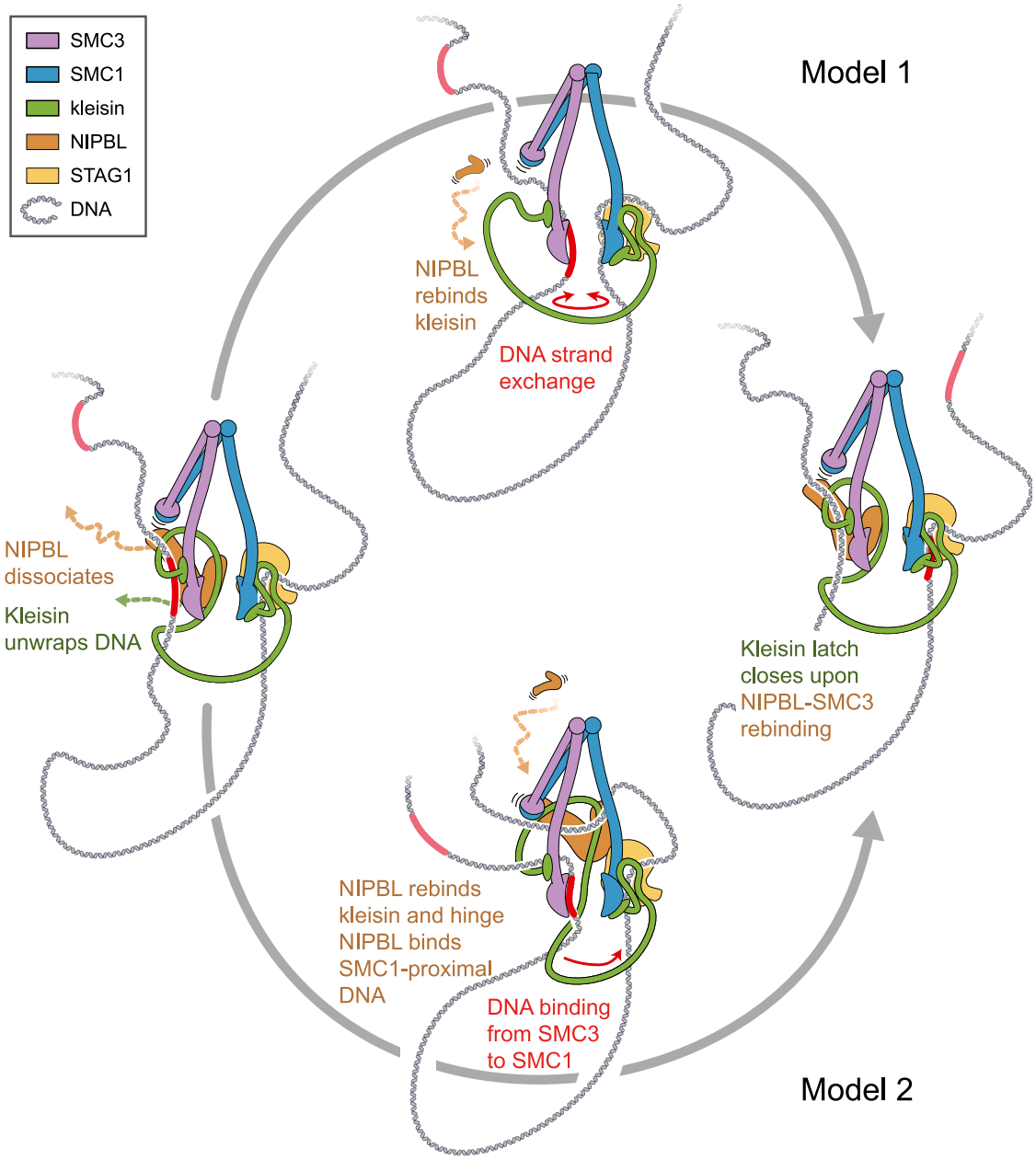

Figure 5. Potential pathways of loop extrusion direction switching via DNA strand exchange mediated by NIPBL exchange

Upon dissociation of NIPBL, the kleisin unwraps DNA (left). To prevent loss of the SMC3-proximal DNA (red), the SMC3 ATPase head binds DNA. DNA may unbind from STAG1-kleisin concomitantly, while the SMC1 ATPase head can bind the SMC1-proximal strand. DNA strand exchange may occur spontaneously between the ATPase heads (upper). Upon rebinding of NIPBL to kleisin (upper) and closing of the kleisin latch, the former SMC1-proximal strand is poised for the next loop extrusion cycle (right). Alternatively, NIPBL may re-bind the cohesin complex by binding to kleisin and the SMC hinge (lower). The NIPBL-kleisin-hinge complex may bind either DNA strand that is the one on which loop extrusion subsequently proceeds. If the former SMC1-proximal DNA strand is chosen, the SMC3-proximal DNA strand exchanges to the DNA-binding site at the SMC1 ATPase head or at STAG1. The binding of NIPBL-kleisin to the SMC3 ATPase head prepares the complex for the next loop extrusion cycle.

See also Figure S6.

Weak DNA binding at the STAG1-kleisin interface could hand over the previously bound DNA strand to a binding site on the SMC1 ATPase head[41] because STAG1 and SMC1 can be positioned in close spatial proximity. Indeed, YCG1 was found in close proximity to both ATPase heads in an ATP-bound state (in the absence of DNA),[51] and a structure prediction by AlphaFold2 (Jumper et al.[52]) suggests that STAG1 may be bound to the SMC1 but not to the SMC3 ATPase head (Figures S6B and

S6C). In the first variant, dissociation of NIPBL could similarly transfer DNA to the DNA-binding site on the SMC3 ATPase head[41] in the ATP-unbound state (Figures 5, upper arc and S6D). The DNA strands can then exchange between the SMC subunits, potentially exploiting the spatial proximity induced by ATPase head engagement upon ATP binding. Rebinding of NIPBL to cohesin selects the SMC3-bound DNA strand as the strand that is subsequently extruded into the loop.

Instead of DNA strand exchange based on the DNA-binding sites on both ATPase heads, a second scenario is that NIPBL could associate with the hinge upon rebinding.[41] In this stage, the NIPBL-hinge complex could bind either the SMC3- or SMC1-proximal DNA strand, poising each one of them to be extruded into the loop in the subsequent extrusion step (Figure S6E). Both possibilities, DNA strand exchange via the DNA-binding sites on the ATPase heads or via NIPBL-hinge association, may or may not lead to DNA strand exchange and require DNA to transiently dissociate from NIPBL and STAG1. This is in line with the observation that NIPBL turnover can, but does not necessarily, lead to direction switching. Strong DNA binding at either HEAT-A or HEAT-B would inhibit these DNA-strand-exchange pathways, explaining why yeast condensin does not undergo direction switches in the presence of the strong safety belt.[2,39] Note that both pathways do not necessarily require subunit exchange, as DNA unbinding from both subunits (and for model 2 unbinding of NIPBL from SMC3 and binding to the hinge) is sufficient. The models are also sufficiently general to be applicable to direction switches observed for human condensin I and II (Kong et al.[10]) as well as for *X. laevis* condensin and cohesin from egg extracts.[5] It is unclear whether ATP binding or hydrolysis contribute to the conformational changes required to enable DNA strand exchange. Because direction switches occur much less frequently than loop extrusion steps, the potential transient states involved in DNA strand exchange are likely difficult to resolve using structural methods like cryoelectron microscopy (cryo-EM).

The physiological relevance of extrusion direction switching

In human and yeast cells, NIPBL is present at a slightly sub-stoichiometric ratio to SCC1 (Holzmann et al.,[53] Huang et al.,[54] Ho et al.,[55] and Cattoglio et al.[56]). However, Pds5 is more abundant than NIPBL, which could potentially result in an excess of NIPBL over Pds5-unbound cohesin *in vivo*. Based on this stoichiometry, we thus expect that NIPBL turnover and direction switching occur *in vivo*, in line with studies that found that SCC2 is not stably associated with chromosomal cohesin[57] and hops between cohesin complexes in HeLa cells.[40] We anticipate that the direction switches described here are essential for proper genome organization by SMC complexes.[58] Simulations have shown that unidirectional extruders are unable to recapitulate the experimentally observed interphase chromosome organization, in particular the formation of TADs, even if the anchor site is only diffusively bound to DNA,[44] whereas asymmetric extrusion with Z-loop formation and direction switching could recapitulate mitotic chromosome formation[44,59] (for direction switching, see also Figure 4A). In contrast, asymmetric extrusion with switching more closely reproduces the stripes and corner dots attributed to CTCF-CTCF loops in interphase chromosome organization. These simulations suggested that cohesin has to undergo direction switches approximately once per minute, yielding in the order of 10 switches before cohesin dissociation from DNA. Indeed, this estimate is in fair agreement with our *in vitro* results (Figure 3B), and adapted simulations using the experimentally observed switching rate *in vitro* support the formation of stripes and CTCF-CTCF dots. Furthermore, upon addition of diffusing and slipping loops to the simulation, extended stripes and dots appear that more closely resemble experimental Hi-C contact maps (Figure 4), suggesting that both direction switching and loop diffusion and slipping occur *in vivo*. Further support that direction switching by cohesin is likely to occur *in vivo* comes from the observation of extrusion "fountains" (in zebrafish[60] and *C. elegans*,[61] "plumes" in mouse cells,[62] and "jets" in mouse thymocytes[63]), regions of enhanced contact frequency in Hi-C maps, which emanate from a narrow region at which cohesin is preferentially loaded and broadening as extrusion proceeds away. Polymer simulations suggest that extrusion direction switching can explain the formation of these fountains.[60] In the simulations, the authors supposed that direction switching resulted from collisions between SMC proteins. However, these results may alternatively (or additionally) be explained by the inherent ability to switch extrusion direction during cohesin-mediated DNA loop extrusion.

Limitations of the study

In experiments that probe the turnover of NIPBL-ΔN, exchanges between NIPBL molecules carrying the same fluorophore faster than 600 ms (two time points) may appear like stably bound complexes. This might potentially account for the fact that not all direction switches were accompanied by a NIPBL exchange in these experiments (Figure 3L) and that direction switches were also observed within periods in which no NIPBL exchange was observed (Figure 3M). Although early experiments demonstrating symmetric DNA loop extrusion by human cohesin were performed under continuous buffer flow,[3] our results suggest that this symmetric extrusion is the result of rapid direction switches with concomitant NIPBL turnover. However, we were unable, within the imaging noise, to observe direction switching at a time resolution of 100 ms and observed only an increase of fluorescence owing to NIPBL at the loop stem and on DNA due to a propensity of NIPBL to accumulate (which is to some extent alleviated by using NIPBL-ΔN), preventing us from observing an exchange of single molecules. Although we identified NIPBL as the key factor underlying direction switching in cohesin, we did not, in the present study, reveal the molecular mechanism underlying direction switches of SMC5/6 and yeast condensin$^{\Delta Ycg1}$.

RESOURCE AVAILABILITY

Lead contact

Further information and requests for resources and reagents should be directed to the lead contact, Cees Dekker (c.dekker@tudelft.nl).

Materials availability

All unique/stable reagents generated in this study are available from the lead contact without restriction.

Data and code availability

- The raw data reported in this study cannot be deposited in a public repository due to its large size. To request access to the full dataset, contact Cees Dekker, TU Delft, (c.dekker@tudelft.nl). A subset of the data that includes raw microscopy data (acquisition time 200 ms per frame) of cohesin-mediated DNA loop extrusion as well as cropped DNA molecules (raw and median-filtered) has been deposited under zenodo (https://zenodo.org/records/13744695; https://doi.org/10.5281/zenodo.12686873) and is publicly available as of the date of publication.
- All original code has been deposited at zenodo repository https://zenodo.org/records/12657734 and is publicly available at https://doi.org/10.5281/zenodo.10420524 as of the date of publication.
- Any additional information required to reanalyze the data reported in this paper is available from the lead contact upon request.

ACKNOWLEDGMENTS

We thank Brian Analikwu and Richard Janissen for discussions and comments on the manuscript and Alejandro Martin Gonzalez, Allard Katan, and Miloš Tišma for discussions. We thank Mathias Madalinski for purifying Atto550- and JF646-HaloTag ligands. The authors acknowledge the use of computational resources of the DelftBlue supercomputer, provided by Delft High Performance Computing Centre (https://www.tudelft.nl/dhpc). Research in the laboratory of C.D. was supported by ERC Advanced Grant 883684 (DNA looping) and the BaSyC program. Research in the laboratory of J.-M.P. was supported by Boehringer Ingelheim, the Austrian Research Promotion Agency (headquarter grant FFG-FO999902549), the European Research Council under the European Union's Horizon 2020 research and innovation program GA no. 101020558, the Human Frontier Science Program (grant RGP0057/2018), and the Vienna Science and Technology Fund (grant LS19-029). J.-M.P. is also an adjunct professor at the Medical University of Vienna. Research in the laboratory of S.G. was supported by ERC Consolidator Grant 724482.

AUTHOR CONTRIBUTIONS

R.B., J.v.d.T., and C.D. designed experiments; R.B. conducted experiments and 3D polymer simulations, analyzed data, and performed AlphaFold2 predictions; I.F.D. purified human cohesin, NIPBL-MAU2, and STAG1, fluorescently labeled NIPBL-ΔN, and established dual-color NIPBL-ΔN imaging; J.v.d.T. made the DNA constructs; M.T. purified yeast SMC5/6; R.B. and C.D. wrote the manuscript with input from all authors; S.G., J.-M.P., and C.D. acquired funding and supervised the work.

DECLARATION OF INTERESTS

The authors declare no competing interests.

STAR★METHODS

Detailed methods are provided in the online version of this paper and include the following:

- KEY RESOURCES TABLE
- EXPERIMENTAL MODEL AND STUDY PARTICIPANT DETAILS
  - Spodoptera frugiperda for expression and purification of human cohesin
  - HeLa Kyoto cells for expression and purification of human cohesin
  - *S. cerevisiae* C5066 for expression and purification of yeast condensin
  - *E. coli* Rosetta (DE3) for expression and purification of SMC5/6 from *E.coli*
  - *S. cerevisiae* strain CB4028 for expression and purification SMC5/6 from yeast
- METHOD DETAILS
  - Protein expression and purification
  - Fluorescent labelling of SMC5/6 and estimation of the labelling efficiency
  - Fluorescent labelling of NIPBL-ΔN
  - Double-tethered DNA assay for single-molecule imaging of DNA loop extrusion
  - Fluorescence Correlation Spectroscopy (FCS)
  - Protein complex structure prediction using AlphaFold2
- QUANTIFICATION AND STATISTICAL ANALYSIS
  - Quantification and segmentation of kymographs
  - Quantification of DNA loop extrusion, loop diffusion, and loop slipping kinetics
  - Bleaching and annotation of NIPBL-ΔN presence
  - Testing the Markov property
  - 3D polymer simulations

SUPPLEMENTAL INFORMATION

Supplemental information can be found online at https://doi.org/10.1016/j.cell.2024.12.020.

Received: December 22, 2023
Revised: September 13, 2024
Accepted: December 13, 2024
Published: January 16, 2025

REFERENCES

1. Kim, E., Barth, R., and Dekker, C. (2023). Looping the Genome with SMC Complexes. Annu. Rev. Biochem. *92*, 15–41. https://doi.org/10.1146/annurev-biochem-032620-110506.
2. Ganji, M., Shaltiel, I.A., Bisht, S., Kim, E., Kalichava, A., Haering, C.H., and Dekker, C. (2018). Real-time imaging of DNA loop extrusion by condensin. Science *360*, 102–105. https://doi.org/10.1126/science.aar7831.
3. Davidson, I.F., Bauer, B., Goetz, D., Tang, W., Wutz, G., and Peters, J.M. (2019). DNA loop extrusion by human cohesin. Science *366*, 1338–1345. https://doi.org/10.1126/science.aaz3418.
4. Kim, Y., Shi, Z., Zhang, H., Finkelstein, I.J., and Yu, H. (2019). Human cohesin compacts DNA by loop extrusion. Science *366*, 1345–1349. https://doi.org/10.1126/science.aaz4475.
5. Golfier, S., Quail, T., Kimura, H., and Brugués, J. (2020). Cohesin and condensin extrude DNA loops in a cell cycle-dependent manner. eLife *9*, e53885. https://doi.org/10.7554/eLife.53885.
6. Higashi, T.L., Pobegalov, G., Tang, M., Molodtsov, M.I., and Uhlmann, F. (2021). A brownian ratchet model for dna loop extrusion by the cohesin complex. eLife *10*, e67530. https://doi.org/10.7554/eLife.67530.
7. Pradhan, B., Kanno, T., Umeda Igarashi, M., Loke, M.S., Baaske, M.D., Wong, J.S.K., Jeppsson, K., Björkegren, C., and Kim, E. (2023). The Smc5/6 complex is a DNA loop-extruding motor. Nature *616*, 843–848. https://doi.org/10.1038/s41586-023-05963-3.
8. Tang, M., Pobegalov, G., Tanizawa, H., Chen, Z.A., Rappsilber, J., Molodtsov, M., Noma, K.I., and Uhlmann, F. (2023). Establishment of dsDNA-dsDNA interactions by the condensin complex. Mol. Cell *83*, 3787–3800.e9. https://doi.org/10.1016/j.molcel.2023.09.019.
9. Janissen, R., Barth, R., Davidson, I.F., Taschner, M., Gruber, S., Peters, J.-M., and Dekker, C. (2024). All eukaryotic SMC proteins induce a twist of -0.6 at each DNA-loop-extrusion step. Preprint at bioRxiv. https://doi.org/10.1101/2024.03.22.586328.
10. Kong, M., Cutts, E.E., Pan, D., Beuron, F., Kaliyappan, T., Xue, C., Morris, E.P., Musacchio, A., Vannini, A., and Greene, E.C. (2020). Human Condensin I and II Drive Extensive ATP-Dependent Compaction of Nucleosome-Bound DNA. Mol. Cell *79*, 99–114.e9. https://doi.org/10.1016/j.molcel.2020.04.026.
11. Ryu, J.-K., Rah, S.-H., Janissen, R., Kerssemakers, J.W.J., Bonato, A., Michieletto, D., and Dekker, C. (2022). Condensin extrudes DNA loops in steps up to hundreds of base pairs that are generated by ATP binding

events. Nucleic Acids Res. *50*, 820–832. https://doi.org/10.1093/nar/gkab1268.

12. Goloborodko, A., Imakaev, M.V., Marko, J.F., and Mirny, L. (2016). Compaction and segregation of sister chromatids via active loop extrusion. eLife *5*, e14864. https://doi.org/10.7554/eLife.14864.
13. Gibcus, J.H., Samejima, K., Goloborodko, A., Samejima, I., Naumova, N., Nuebler, J., Kanemaki, M.T., Xie, L., Paulson, J.R., Earnshaw, W.C., et al. (2018). A pathway for mitotic chromosome formation. Science *359*, eaao6135. https://doi.org/10.1126/science.aao6135.
14. de Wit, E., Vos, E.S.M., Holwerda, S.J.B., Valdes-Quezada, C., Verstegen, M.J.A.M., Teunissen, H., Splinter, E., Wijchers, P.J., Krijger, P.H.L., and de Laat, W. (2015). CTCF Binding Polarity Determines Chromatin Looping. Mol. Cell *60*, 676–684. https://doi.org/10.1016/j.molcel.2015.09.023.
15. Davidson, I.F., Barth, R., Zaczek, M., Van Der Torre, J., Tang, W., Nagasaka, K., Janissen, R., Kerssemakers, J., Wutz, G., Dekker, C., et al. (2023). CTCF is a DNA-tension-dependent barrier to cohesin-mediated loop extrusion. Nature *616*, 822–827. https://doi.org/10.1038/s41586-023-05961-5.
16. Guo, Y., Xu, Q., Canzio, D., Shou, J., Li, J., Gorkin, D.U., Jung, I., Wu, H., Zhai, Y., Tang, Y., et al. (2015). CRISPR Inversion of CTCF Sites Alters Genome Topology and Enhancer/Promoter Function. Cell *162*, 900–910. https://doi.org/10.1016/j.cell.2015.07.038.
17. Li, Y., Haarhuis, J.H.I., Sedeño Cacciatore, Á., Oldenkamp, R., van Ruiten, M.S., Willems, L., Teunissen, H., Muir, K.W., de Wit, E., Rowland, B.D., et al. (2020). The structural basis for cohesin–CTCF-anchored loops. Nature *578*, 472–476. https://doi.org/10.1038/s41586-019-1910-z.
18. Wutz, G., Várnai, C., Nagasaka, K., Cisneros, D.A., Stocsits, R.R., Tang, W., Schoenfelder, S., Jessberger, G., Muhar, M., Hossain, M.J., et al. (2017). Topologically associating domains and chromatin loops depend on cohesin and are regulated by CTCF, WAPL, and PDS5 proteins. EMBO J. *36*, 3573–3599. https://doi.org/10.15252/embj.201798004.
19. Nora, E.P., Lajoie, B.R., Schulz, E.G., Giorgetti, L., Okamoto, I., Servant, N., Piolot, T., Van Berkum, N.L., Meisig, J., Sedat, J., et al. (2012). Spatial partitioning of the regulatory landscape of the X-inactivation centre. Nature *485*, 381–385. https://doi.org/10.1038/nature11049.
20. Nora, E.P., Goloborodko, A., Valton, A.L., Gibcus, J.H., Uebersohn, A., Abdennur, N., Dekker, J., Mirny, L.A., and Bruneau, B.G. (2017). Targeted Degradation of CTCF Decouples Local Insulation of Chromosome Domains from Genomic Compartmentalization. Cell *169*, 930–944.e22. https://doi.org/10.1016/j.cell.2017.05.004.
21. Rao, S.S.P., Huntley, M.H., Durand, N.C., Stamenova, E.K., Bochkov, I.D., Robinson, J.T., Sanborn, A.L., Machol, I., Omer, A.D., Lander, E.S., et al. (2014). A 3D map of the human genome at kilobase resolution reveals principles of chromatin looping. Cell *159*, 1665–1680. https://doi.org/10.1016/j.cell.2014.11.021.
22. Rao, S.S.P., Huang, S.C., Glenn St Hilaire, B., Engreitz, J.M., Perez, E.M., Kieffer-Kwon, K.R., Sanborn, A.L., Johnstone, S.E., Bascom, G.D., Bochkov, I.D., et al. (2017). Cohesin Loss Eliminates All Loop Domains. Cell *171*, 305–320.e24. https://doi.org/10.1016/j.cell.2017.09.026.
23. Vietri Rudan, M., Barrington, C., Henderson, S., Ernst, C., Odom, D.T., Tanay, A., and Hadjur, S. (2015). Comparative Hi-C Reveals that CTCF Underlies Evolution of Chromosomal Domain Architecture. Cell Rep. *10*, 1297–1309. https://doi.org/10.1016/j.celrep.2015.02.004.
24. Hansen, A.S., Cattoglio, C., Darzacq, X., and Tjian, R. (2018). Recent evidence that TADs and chromatin loops are dynamic structures. Nucleus *9*, 20–32. https://doi.org/10.1080/19491034.2017.1389365.
25. Gabriele, M., Brandão, H.B., Grosse-Holz, S., Jha, A., Dailey, G.M., Cattoglio, C., Hsieh, T.H.S., Mirny, L., Zechner, C., and Hansen, A.S. (2022). Dynamics of CTCF- and cohesin-mediated chromatin looping revealed by live-cell imaging. Science *376*, 476–501. https://doi.org/10.1126/science.abn6583.
26. Mach, P., Kos, P.I., Zhan, Y., Cramard, J., Gaudin, S., Tünnermann, J., Marchi, E., Eglinger, J., Zuin, J., Kryzhanovska, M., et al. (2022). Cohesin and CTCF control the dynamics of chromosome folding. Nat. Genet. *54*, 1907–1918. https://doi.org/10.1038/s41588-022-01232-7.
27. Horsfield, J.A. (2023). Full circle: a brief history of cohesin and the regulation of gene expression. FEBS J. *290*, 1670–1687. https://doi.org/10.1111/febs.16362.
28. Arnould, C., Rocher, V., Finoux, A.L., Clouaire, T., Li, K., Zhou, F., Caron, P., Mangeot, P.E., Ricci, E.P., Mourad, R., et al. (2021). Loop extrusion as a mechanism for formation of DNA damage repair foci. Nature *590*, 660–665. https://doi.org/10.1038/s41586-021-03193-z.
29. Litwin, I., Pilarczyk, E., and Wysocki, R. (2018). The Emerging Role of Cohesin in the DNA Damage Response. Genes *9*, 581. https://doi.org/10.3390/genes9120581.
30. Phipps, J., Nasim, A., and Miller, D.R. (1985). Recovery, Repair, and Mutagenesis in Schizosaccharomyces pombe. In Advances in Genetices, *23* (Elsevier), pp. 1–72. https://doi.org/10.1016/S0065-2660(08)60511-8.
31. Aragón, L. (2018). The Smc5/6 Complex: New and Old Functions of the Enigmatic Long-Distance Relative. Annu. Rev. Genet. *52*, 89–107. https://doi.org/10.1146/annurev-genet-120417-031353.
32. McDonald, W.H., Pavlova, Y., Yates, J.R., and Boddy, M.N. (2003). Novel Essential DNA Repair Proteins Nse1 and Nse2 Are Subunits of the Fission Yeast Smc5-Smc6 Complex. J. Biol. Chem. *278*, 45460–45467. https://doi.org/10.1074/jbc.M308828200.
33. Bürmann, F., and Löwe, J. (2023). Structural biology of SMC complexes across the tree of life. Curr. Opin. Struct. Biol. *80*, 102598. https://doi.org/10.1016/j.sbi.2023.102598.
34. Datta, S., Lecomte, L., and Haering, C.H. (2020). Structural insights into DNA loop extrusion by SMC protein complexes. Curr. Opin. Struct. Biol. *65*, 102–109. https://doi.org/10.1016/j.sbi.2020.06.009.
35. Oldenkamp, R., and Rowland, B.D. (2022). A walk through the SMC cycle: from catching DNAs to shaping the genome. Mol. Cell *82*, 1616–1630. https://doi.org/10.1016/j.molcel.2022.04.006.
36. Shaltiel, I.A., Datta, S., Lecomte, L., Hassler, M., Kschonsak, M., Bravo, S., Stober, C., Ormanns, J., Eustermann, S., and Haering, C.H. (2022). A hold-and-feed mechanism drives directional DNA loop extrusion by condensin. Science *376*, 1087–1094. https://doi.org/10.1126/science.abm4012.
37. Dekker, C., Haering, C.H., Peters, J.-M., and Rowland, B.D. (2023). How do molecular motors fold the genome? Science *382*, 646–648. https://doi.org/10.1126/science.adi8308.
38. Taschner, M., and Gruber, S. (2023). DNA segment capture by Smc5/6 holocomplexes. Nat. Struct. Mol. Biol. *30*, 619–628. https://doi.org/10.1038/s41594-023-00956-2.
39. Kschonsak, M., Merkel, F., Bisht, S., Metz, J., Rybin, V., Hassler, M., and Haering, C.H. (2017). Structural Basis for a Safety-Belt Mechanism That Anchors Condensin to Chromosomes. Cell *171*, 588–600.e24. https://doi.org/10.1016/j.cell.2017.09.008.
40. Rhodes, J., Mazza, D., Nasmyth, K., and Uphoff, S. (2017). Scc2/Nipbl hops between chromosomal cohesin rings after loading. eLife *6*, e30000. https://doi.org/10.7554/eLife.30000.
41. Bauer, B.W., Davidson, I.F., Canena, D., Wutz, G., Tang, W., Litos, G., Horn, S., Hinterdorfer, P., and Peters, J.M. (2021). Cohesin mediates DNA loop extrusion by a "swing and clamp" mechanism. Cell *184*, 5448–5464.e22. https://doi.org/10.1016/j.cell.2021.09.016.
42. Shi, Z., Gao, H., Bai, X.C., and Yu, H. (2020). Cryo-EM structure of the human cohesin-NIPBL-DNA complex. Science *368*, 1454–1459. https://doi.org/10.1126/science.abb0981.
43. Collier, J.E., Lee, B.G., Roig, M.B., Yatskevich, S., Petela, N.J., Metson, J., Voulgaris, M., Gonzalez Llamazares, A.G., Löwe, J., and Nasmyth, K.A. (2020). Transport of DNA within cohesin involves clamping on top of engaged heads by SCC2 and entrapment within the ring by SCC3. eLife *9*, e59560. https://doi.org/10.7554/eLife.59560.
44. Banigan, E.J., van den Berg, A.A., Brandão, H.B., Marko, J.F., and Mirny, L.A. (2020). Chromosome organization by one-sided and two-sided loop extrusion. eLife *9*, e53558. https://doi.org/10.7554/eLife.53558.

45. Kerpedjiev, P., Abdennur, N., Lekschas, F., McCallum, C., Dinkla, K., Strobelt, H., Luber, J.M., Ouellette, S.B., Azhir, A., Kumar, N., et al. (2018). HiGlass: web-based visual exploration and analysis of genome interaction maps. Genome Biol. *19*, 125. https://doi.org/10.1186/s13059-018-1486-1.

46. Davidson, I.F., and Peters, J.M. (2021). Genome folding through loop extrusion by SMC complexes. Nat. Rev. Mol. Cell Biol. *22*, 445–464. https://doi.org/10.1038/s41580-021-00349-7.

47. Bastié, N., Chapard, C., Dauban, L., Gadal, O., Beckouët, F., and Koszul, R. (2022). Smc3 acetylation, Pds5 and Scc2 control the translocase activity that establishes cohesin-dependent chromatin loops. Nat. Struct. Mol. Biol. *29*, 575–585. https://doi.org/10.1038/s41594-022-00780-0.

48. Petela, N.J., Gligoris, T.G., Metson, J., Lee, B.-G., Voulgaris, M., Hu, B., Kikuchi, S., Chapard, C., Chen, W., Rajendra, E., et al. (2018). Scc2 Is a Potent Activator of Cohesin's ATPase that Promotes Loading by Binding Scc1 without Pds5. Mol. Cell *70*, 1134–1148.e7. https://doi.org/10.1016/j.molcel.2018.05.022.

49. Van Ruiten, M.S., Van Gent, D., Sedeño Cacciatore, Á., Fauster, A., Willems, L., Hekkelman, M.L., Hoekman, L., Altelaar, M., Haarhuis, J.H.I., Brummelkamp, T.R., et al. (2022). The cohesin acetylation cycle controls chromatin loop length through a PDS5A brake mechanism. Nat. Struct. Mol. Biol. *29*, 586–591. https://doi.org/10.1038/s41594-022-00773-z.

50. Bastié, N., Chapard, C., Cournac, A., Nejmi, S., Mboumba, H., Gadal, O., Thierry, A., Beckouët, F., and Koszul, R. (2024). Sister chromatid cohesion halts DNA loop expansion. Mol. Cell *84*, 1139–1148.e5. https://doi.org/10.1016/j.molcel.2024.02.004.

51. Lee, B.G., Merkel, F., Allegretti, M., Hassler, M., Cawood, C., Lecomte, L., O'Reilly, F.J., Sinn, L.R., Gutierrez-Escribano, P., Kschonsak, M., et al. (2020). Cryo-EM structures of holo condensin reveal a subunit flip-flop mechanism. Nat. Struct. Mol. Biol. *27*, 743–751. https://doi.org/10.1038/s41594-020-0457-x.

52. Jumper, J., Evans, R., Pritzel, A., Green, T., Figurnov, M., Ronneberger, O., Tunyasuvunakool, K., Bates, R., Žídek, A., Potapenko, A., et al. (2021). Highly accurate protein structure prediction with AlphaFold. Nature *596*, 583–589. https://doi.org/10.1038/s41586-021-03819-2.

53. Holzmann, J., Politi, A.Z., Nagasaka, K., Hantsche-Grininger, M., Walther, N., Koch, B., Fuchs, J., Dürnberger, G., Tang, W., Ladurner, R., et al. (2019). Absolute quantification of cohesin, CTCF and their regulators in human cells. eLife *8*, e46269. https://doi.org/10.7554/eLife.46269.

54. Huang, Q., Szklarczyk, D., Wang, M., Simonovic, M., and Von Mering, C. (2023). PaxDb 5.0: Curated Protein Quantification Data Suggests Adaptive Proteome Changes in Yeasts. Mol. Cell. Proteomics *22*, 100640. https://doi.org/10.1016/j.mcpro.2023.100640.

55. Ho, B., Baryshnikova, A., and Brown, G.W. (2018). Unification of Protein Abundance Datasets Yields a Quantitative Saccharomyces cerevisiae Proteome. Cell Syst. *6*, 192–205.e3. https://doi.org/10.1016/j.cels.2017.12.004.

56. Cattoglio, C., Pustova, I., Walther, N., Ho, J.J., Hantsche-Grininger, M., Inouye, C.J., Hossain, M.J., Dailey, G.M., Ellenberg, J., Darzacq, X., et al. (2019). Determining cellular CTCF and cohesin abundances to constrain 3D genome models. eLife *8*, e40164. https://doi.org/10.7554/eLife.40164.

57. Hu, B., Itoh, T., Mishra, A., Katoh, Y., Chan, K.-L., Upcher, W., Godlee, C., Roig, M.B., Shirahige, K., and Nasmyth, K. (2011). ATP Hydrolysis Is Required for Relocating Cohesin from Sites Occupied by Its Scc2/4 Loading Complex. Curr. Biol. *21*, 12–24. https://doi.org/10.1016/j.cub.2010.12.004.

58. Fudenberg, G., Abdennur, N., Imakaev, M., Goloborodko, A., and Mirny, L.A. (2017). Emerging Evidence of Chromosome Folding by Loop Extrusion. Cold Spring Harb. Symp. Quant. Biol. *82*, 45–55. https://doi.org/10.1101/sqb.2017.82.034710.

59. Dey, A., Shi, G., Takaki, R., and Thirumalai, D. (2023). Structural changes in chromosomes driven by multiple condensin motors during mitosis. Cell Rep. *42*, 112348. https://doi.org/10.1016/j.celrep.2023.112348.

60. Galitsyna, A., Ulianov, S.V., Bykov, N.S., Veil, M., Gao, M., Perevoschikova, K., Gelfand, M., Razin, S.V., Mirny, L., and Onichtchouk, D. (2023). Extrusion fountains are hallmarks of chromosome organization emerging upon zygotic genome activation. Preprint at bioRxiv. https://doi.org/10.1101/2023.07.15.549120.

61. Isiaka, B.N., Semple, J.I., Haemmerli, A., Thapliyal, S., Stojanovski, K., Das, M., Gilbert, N., Glauser, D.A., Towbin, B., Jost, D., et al. (2023). Cohesin forms fountains at active enhancers in C. elegans. Preprint at bioRxiv. https://doi.org/10.1101/2023.07.14.549011.

62. Liu, N.Q., Magnitov, M., Schijns, M., Van Schaik, T., Van Der Weide, R.H., Teunissen, H., Van Steensel, B., and De Wit, E. (2021). Rapid depletion of CTCF and cohesin proteins reveals dynamic features of chromosome architecture. Preprint at bioRxiv. https://doi.org/10.1101/2021.08.27.457977.

63. Guo, Y., Al-Jibury, E., Garcia-Millan, R., Ntagiantas, K., King, J.W.D., Nash, A.J., Galjart, N., Lenhard, B., Rueckert, D., Fisher, A.G., et al. (2022). Chromatin jets define the properties of cohesin-driven in vivo loop extrusion. Mol. Cell *82*, 3769–3780.e5. https://doi.org/10.1016/j.molcel.2022.09.003.

64. Hassler, M., Shaltiel, I.A., Kschonsak, M., Simon, B., Merkel, F., Thärichen, L., Bailey, H.J., Macošek, J., Bravo, S., Metz, J., et al. (2019). Structural Basis of an Asymmetric Condensin ATPase Cycle. Mol. Cell *74*, 1175–1188.e9. https://doi.org/10.1016/j.molcel.2019.03.037.

65. Taschner, M., Basquin, J., Steigenberger, B., Schäfer, I.B., Soh, Y.M., Basquin, C., Lorentzen, E., Räschle, M., Scheltema, R.A., and Gruber, S. (2021). Nse5/6 inhibits the Smc5/6 ATPase and modulates DNA substrate binding. EMBO J. *40*, e107807. https://doi.org/10.15252/embj.2021107807.

66. Edelstein, D.A., Tsuchida, A.M., Amodaj, N., Pinkard, H., Vale, D.R., and Stuurman, N. (2014). Advanced methods of microscope control using μManager software. J. Biol. Methods *1*, e10. https://doi.org/10.14440/jbm.2014.36.

67. Schrimpf, W., Barth, A., Hendrix, J., and Lamb, D.C. (2018). PAM: A Framework for Integrated Analysis of Imaging, Single-Molecule, and Ensemble Fluorescence Data. Biophys. J. *114*, 1518–1528. https://doi.org/10.1016/j.bpj.2018.02.035.

68. Mirdita, M., Schütze, K., Moriwaki, Y., Heo, L., Ovchinnikov, S., and Steinegger, M. (2022). ColabFold: making protein folding accessible to all. Nat. Methods *19*, 679–682. https://doi.org/10.1038/s41592-022-01488-1.

69. Kim, E., Gonzalez, A.M., Pradhan, B., van der Torre, J., and Dekker, C. (2022). Condensin-driven loop extrusion on supercoiled DNA. Nat. Struct. Mol. Biol. *29*, 719–727. https://doi.org/10.1038/s41594-022-00802-x.

70. Kim, E., Kerssemakers, J., Shaltiel, I.A., Haering, C.H., and Dekker, C. (2020). DNA-loop extruding condensin complexes can traverse one another. Nature *579*, 438–442. https://doi.org/10.1038/s41586-020-2067-5.

71. Pradhan, B., Barth, R., Kim, E., Davidson, I.F., Bauer, B., van Laar, T., Yang, W., Ryu, J.-K., van der Torre, J., Peters, J.-M., et al. (2022). SMC complexes can traverse physical roadblocks bigger than their ring size. Cell Rep. *41*, 111491. https://doi.org/10.1016/j.celrep.2022.111491.

72. Park, S.R., Hauver, J., Zhang, Y., Revyakin, A., Coleman, R.A., Tjian, R., Chu, S., and Pertsinidis, A. (2020). A Single-Molecule Surface-Based Platform to Detect the Assembly and Function of the Human RNA Polymerase II Transcription Machinery. Structure *28*, 1337–1343.e4. https://doi.org/10.1016/j.str.2020.07.009.

73. Jeppsson, K., Pradhan, B., Sutani, T., Sakata, T., Igarashi, M.U., Berta, D.G., Kanno, T., Nakato, R., Shirahige, K., Kim, E., et al. (2023). Loop-extruding Smc5/6 organizes transcription-induced positive DNA supercoils. Mol. Cell *84*, 867–882.e5. https://doi.org/10.1101/2023.06.20.545053.

74. Martínez-García, B., Dyson, S., Segura, J., Ayats, A., Cutts, E.E., Gutierrez-Escribano, P., Aragón, L., and Roca, J. (2023). Condensin pinches a short negatively supercoiled DNA loop during each round

of ATP usage. EMBO J. *42*, e111913. https://doi.org/10.15252/embj.2022111913.

75. Kimura, K., and Hirano, T. (1997). ATP-dependent positive supercoiling of DNA by 13S condensin: A biochemical implication for chromosome condensation. Cell *90*, 625–634. https://doi.org/10.1016/S0092-8674(00)80524-3.
76. Kapusta, P. (2010). Absolute diffusion coefficients: compilation of reference data for FCS calibration.
77. Goddard, T.D., Huang, C.C., Meng, E.C., Pettersen, E.F., Couch, G.S., Morris, J.H., and Ferrin, T.E. (2018). UCSF ChimeraX: Meeting modern challenges in visualization and analysis. Protein Sci. *27*, 14–25. https://doi.org/10.1002/pro.3235.
78. Virtanen, P., Gommers, R., Oliphant, T.E., Haberland, M., Reddy, T., Cournapeau, D., Burovski, E., Peterson, P., Weckesser, W., Bright, J., et al. (2020). SciPy 1.0: fundamental algorithms for scientific computing in Python. Nat. Methods *17*, 261–272. https://doi.org/10.1038/s41592-019-0686-2.
79. Truong, C., Oudre, L., and Vayatis, N. (2020). Selective review of offline change point detection methods. Signal Process. *167*, 107299. https://doi.org/10.1016/j.sigpro.2019.107299.
80. Liu, H., and Shima, T. (2021). A fast and objective hidden Markov modeling for accurate analysis of biophysical data with numerous states. Preprint at bioRxiv. https://doi.org/10.1101/2021.05.30.446337.
81. Kemeny, J.G., and Snell, J.L. (1960). Finite Markov Chains (Van Nostrand).
82. Anderson, T.W., and Goodman, L.A. (1957). Statistical Inference about Markov Chains. Ann. Math. Statist. *28*, 89–110. https://doi.org/10.1214/aoms/1177707039.
83. Delft High Performance Computing Centre (2024). DelftBlue Supercomputer (Phase 2). https://www.tudelft.nl/dhpc.

STAR★METHODS

KEY RESOURCES TABLE

REAGENT or RESOURCE	SOURCE	IDENTIFIER
Bacterial and virus strains		
E. coli Rosetta (DE3)	Novagen	70954
Chemicals, peptides, and recombinant proteins		
Fetal calf serum	Thermo Fisher Scientific	A5256801
L-glutamine	Thermo Fisher Scientific	25030-024
Penicillin/Streptomycin	Sigma	P0781
Yeast nitrogen base	Difco	BD 291940
Casamino acids	Difco	BD 228830
Leucine	Sigma	L8000
Tyrosine	Sigma	T3754
Adenine	Sigma	A8626
D-glucose	Sigma	G8270
D-raffinose	Biosynth	R-1000
D-galactose	Biosynth	G-1700
StrepTrap HP 5 ml	Cytiva	28-9075-47
HiTrap Heparin 5 ml	Cytiva	17040701
Superose 6 Increase 10/300 GL	Cytiva	29091596
d-Desthiobiotin, 500 mg	Sigma	D1411
IgG Sepharose FastFlow	Cytiva	17096901
JF646 HALO ligand	Promega	GA1120
SNAP-Surface AlexaFluor 647	NEB	S9136S
C2-maleimide AlexaFluor 647	Thermo Fisher Scientific	10144342
Zeba Spin Desalting Columns, 7K MWCO, 0.5 ml	Thermo Fisher Scientific	89882
APTES ((3-Aminopropyl)trimethoxysilane)	Sigma	281778
Methyl-PEG4-NHS Esther	Fisher Scientific	22341
Biotin-PEG-SVA, MW 5000	Laysan Bio	Biotin-PEG-SVA-5000
MPEG-SVA-5000	Laysan Bio	MPEG-SVA-5000
ATP	Thermo Fisher Scientific	10304340
DTT	Thermo Fisher Scientific	10448730
TCEP	Thermo Fisher Scientific	10530434
SYTOX Orange	Invitrogen	10338062
SYTOX Green	Thermo Fisher Scientific	10768273
Halo Ligand Amine O2	Promega	P6711
JF646 SE	Tocris	6148
ATTO 550 NHS-ester	ATTO-TEC	AD 550-35
Toyopearl AF-Chelate-650M	Tosoh	0014475
Flag M2 agarose beads	Sigma	A2220-25ML
Sephacryl S-1000 Superfine	Cytiva	No longer sold
cOmplete EDTA-free protease inhibitor	Roche	11873580001
Strep-Tactin Superflow high capacity resin	IBA	2-1208-010
Desthiobiotin	Merck Sigma	D1411
5-mL HisTrap column	Cytiva	17524801
Superose 6 column	Cytiva	29091596
Streptavidin	Thermo Fisher Scientific	10700995

(*Continued on next page*)

Continued

REAGENT or RESOURCE	SOURCE	IDENTIFIER
Superdex200 Increase 10/300 GL SEC column	Cytiva	28990944
Bennzonase	Merck	70664
Trolox ((±)-6-Hydroxy-2,5,7,8-tetramethylchromane-2-carboxylic acid)	Sigma	238813
Glucose oxidase	Fisher Scientific	11491092
Catalase from bovine liver	Sigma	C30
BSA	Thermo Fisher Scientific	10536735
Taq DNA ligase	NEB	M0208
Human cohesin from *Sf9* insect cells	Davidson et al.[3]; this study	N/A
Human cohesin from HeLa cells	Davidson et al.[3]; this study	N/A
NIPBL-Mau2	Davidson et al.[3]; this study	N/A
NIPBL-DN	Bauer et al.[41]; this study	N/A
Yeast condensing	Ganji et al.[2]; Hassler et al.[64]; this study	N/A
Yeast SMC5/6 purifiied from *E.coli*	Taschner and Gruber[38] and Taschner et al.[65]; this study	N/A
Yeast SMC5/6 purified from yeast	Pradhan et al.[7]; this study	N/A
NSE5/6	Taschner and Gruber[38] and Taschner et al.[65]; this study	N/A
Deposited data		
Hi-C contact matrix of the HOXA locus	Li et al.[17]	GSE126637
Experimental models: Cell lines		
Spodoptera frugiperda	Thermo Fisher Scientific	B82501
Hela SCC1-HALO-FLAG	Davidson et al.[3]	N/A
S. cerevisiae strain CB4028	Pradhan et al.[7]	N/A
S. cerevisiae C5066	Hassler et al.[64]	N/A
Oligonucleotides		
5'-GGGCGGCGACCT-3'Biotin	This study	N/A
5'- AGGTCGCCGCCC-3'Biotin	This study	N/A
Recombinant DNA		
λ-DNA	NEB	N3011
Cohesin expression plasmid (pBig2ab SMC1, SMC3-FLAG, SCC1(TEV)-HALO, HIS-STAG1; c136)	Davidson et al.[3]	N/A
NIPBL-MAU2 expression plasmid (pLib FLAG-HALO-NIPBL, MAU2; LC50A)	Davidson et al.[3]	N/A
NIPBL-ΔN expression plasmid (pLib FLAG-HALO-NIPBL(Δ22-1040); BB17/241)	Bauer et al.[41]	N/A
Software and algorithms		
Fiji version 1.54i	NIH	N/A
Python version 3.7.7	Python Software Foundation	https://www.python.org
Prism version 9	GraphPad	N/A
μManager version 2.0	Edelstein et al.[66]	https://github.com/micro-manager
Illustrator version 28.5	Adobe	N/A
Symphotime 64	PicoQuant	N/A
PAM	Schrimpf et al.[67]	https://gitlab.com/PAM-PIE
AlphaFold-Multimer using ColabFold v1.5.5	Mirdita et al.[68]	https://github.com/sokrypton/ColabFold
Custom code	This study	https://doi.org/10.5281/zenodo.10420524

(*Continued on next page*)

Continued

REAGENT or RESOURCE	SOURCE	IDENTIFIER
Polymer simulation code	Banigan et al.[44]; this study	https://github.com/mirnylab/one_sided_extrusion
Other		
Vivaspin 20 (100 kDa MWCO) ultrafiltration units	Sartorius	VS2042
Vivaspin 6 (100 kDa MWCO) ultrafiltration units	Sartorius	VS0642
Amicon Ultra Centrifugal filter (50 kDa MWCO)	Sigma	UFC9050

EXPERIMENTAL MODEL AND STUDY PARTICIPANT DETAILS

Spodoptera frugiperda for expression and purification of human cohesin

Cultures were harvested after 48 – 60 h expression at 27 °C, washed in PBS, frozen in liquid nitrogen and stored at -80°C until use.[3]

HeLa Kyoto cells for expression and purification of human cohesin

HeLa Kyoto cells were cultured at 37 °C, 5 % CO_2 in DMEM (prepared in-house) supplemented with 10% fetal calf serum (A5256801; Thermo Fisher), 0.2 mM L-glutamine (25030-024; Thermo Fisher), and 1x Penicillin/Streptomycin (P0781; Sigma-Aldrich).[3,18]

S. cerevisiae C5066 for expression and purification of yeast condensin

A 5-fold stock of -URA-TRP was prepared with 40 g/L yeast nitrogen base (Difco BD 291940), 18 g/L casamino acids (Difco BD 228830), 500 mg/L leucine (Merck Sigma L8000), 275 mg/L tyrosine (Merck Sigma T3754), and 275 mg/L adenine (Merck Sigma A8626). With the exception of leucine that was filter-sterilized, all components were autoclaved. For one condensin purification, 0.5 L of preculture was grown on -URA-TRP medium supplemented with 2 g/l D-glucose (Merck Sigma G8270), 6 L of main culture on -URA-TRP supplemented with 2 g/l D-raffinose (Biosynth R-1000), and condensin expression was induced by adding 2 g/l D-galactose (Biosynth G-1700) when the OD_{600} reaches ~1.0, and continued overnight for 12-14 hours, yielding around 50 g of cells. Cultures are grown at 30 °C with vigorous shaking (180 rpm).

E. coli Rosetta (DE3) for expression and purification of SMC5/6 from *E.coli*

1 liter of the strain was grown in Terrific Broth medium at 37 °C to an OD_{600} of 1.0 and the culture temperature was reduced to 22 °C. Expression was then induced with isopropyl β-d-1-thiogalactopyranoside at a final concentration of 0.4 mM and allowed to proceed overnight (typically for 16 h).

S. cerevisiae strain CB4028 for expression and purification SMC5/6 from yeast

Overexpression strains were grown at 30 °C in YEP-lactate medium to optical density (OD_{600}) 0.8–1.0. Protein expression was induced for 4 h by the addition of 2% galactose.

METHOD DETAILS

Protein expression and purification

Human cohesin, as well as NIPBL-MAU2, were expressed in and purified from *Sf9* insect cells and HeLa cells as described previously.[3] All steps were carried out at 4°C unless indicated otherwise. For cohesin and NIPBL-Mau2 purified from *Sf9* insect cells, cell pellets were lysed using Dounce homogenization in recombinant cohesin purification buffer 1 (25 mM NaH_2PO_4/Na_2HPO_4, pH 7.5; 500 mM NaCl; 5% glycerol) with added 10 mM imidazole, pH 7.5, 0.05% Tween 20, 1 mM PMSF, 3 mM beta-mercaptoethanol, 10 μg/ml aprotinin, 2 mM benzamidine (Sigma), and cOmplete EDTA-free protease inhibitor cocktail. Following centrifugation at 48,000 g for 45 minutes, the supernatant was mixed with 5 ml of Toyopearl AF-chelate-650M resin (Tosoh Bioscience) pre-charged with Ni2+ ions and incubated for 3 hours. The beads were washed with three rounds of 10 bead volumes of recombinant cohesin purification buffer 1, supplemented with 15 mM imidazole, pH 7.5, and 0.01% Tween 20. Bound protein was eluted with 25 ml of recombinant cohesin purification buffer 2 (25 mM NaH_2PO_4/Na_2HPO_4, pH 7.5; 150 mM NaCl; 5% glycerol; 300 mM imidazole, pH 7.5; 0.01% Tween 20). The eluate was combined with 5 ml of FLAG-M2 agarose resin (Sigma; A2220) and incubated for three hours. The beads were washed with three rounds of 10 bead volumes of cohesin purification buffer 3 (25 mM NaH_2PO_4/Na_2HPO_4, pH 7.5; 150 mM NaCl; 5% glycerol; 50 mM imidazole, pH 7.5). To label recombinant cohesin^{STAG1} fluorescently, FLAG-M2 agarose beads were resuspended to one bead volume in recombinant cohesin purification buffer 3, supplemented with excess JF646-HaloTag ligand and incubated for 15 min at room temperature protected from light.

To prepare JF646-HaloTag, 1 mg of Janelia Fluor 646 SE (Tocris; 6148) was dissolved in 200 μl of dimethylformamide (DMF). Separately, 5 mg of HaloTag Amine (O2) Ligand (Promega; P6711) was dissolved in DMF to a concentration of ~120 mM. Then, 50 μl of the HaloTag Amine (O2) Ligand solution was added dropwise to 200 μl of Janelia Fluor 646 SE while mixing. Next, 10 μl of

diisopropylethylamine (Sigma) was added, and the reaction was incubated at room temperature for ~16 hours, protected from light. The reaction mixture was then diluted 10-fold in solvent A (5% acetonitrile, 0.1% formic acid) and purified through five successive reverse phase HPLC runs using an Ultimate 3000 (ThermoFisher Scientific) equipped with a Kinetex 5 μm XBC18 100A, 250 x 4.6 mm column. The solvents used were solvent A (5% acetonitrile, 0.1% formic acid) and solvent B (acetonitrile, 0.1% formic acid), with a gradient from 0% to 100% B over 30 minutes at a flow rate of 0.8 ml/min. Peak fractions were pooled, lyophilized, re-suspended in DMSO, frozen in liquid nitrogen, and stored at -80°C. After the labeling reaction, the beads were extensively washed with recombinant cohesin purification buffer 3.

Bound protein was eluted with 25 ml of recombinant cohesin purification buffer 3, supplemented with 0.5 mg/ml 3xFLAG peptide. Eluates were concentrated to approximately 0.5 ml using Vivaspin 20 (100 kDa MWCO) ultrafiltration units (Sartorius; VS2042), frozen in liquid nitrogen, and stored at -80°C.

Recombinant cohesin from *Sf9* insect cells was fluorescently labelled with a labelling efficiency of 84 ± 6 % (N = 6; measured analogous to SMC5/6, see below).

For cohesin from HeLa cells, a cell pellet was thawed and resuspended in 40 ml of HeLa cohesin purification buffer 1 (20 mM Tris, pH 7.5; 1.5 mM MgCl2; 10 mM KCl) supplemented with 1 mM DTT, 1 mM PMSF, and cOmplete EDTA-free protease inhibitor cocktail (Roche; 11873580001). Cells were lysed using 10 strokes of Dounce homogenization, incubated on ice for 10 minutes, and then homogenized for another 15 strokes. Nuclei were pelleted by centrifugation at 2000 rpm for 15 minutes.

The pelleted nuclei were resuspended in 36 ml of HeLa purification buffer 1 with 1 mM DTT and 1 mM PMSF and homogenized with 3 strokes. NaCl was added to a final concentration of 500 mM dropwise while stirring. Tween 20 was then added to 0.1%, and the lysate was stirred for 10 minutes before sonication (Branson Digital Sonifier; 60 x 0.5 s pulses at 40% amplitude). Following centrifugation at 48,000 g for 30 minutes, the soluble fraction was combined with 1 ml of FLAG-M2 agarose resin and incubated for three hours.

Beads were washed with 10 bead volumes of HeLa cohesin purification buffer 2 (25 mM NaH_2PO_4/Na_2HPO_4, pH 7.5; 500 mM NaCl; 5% glycerol; 1 mM EDTA) and three rounds of 10 bead volumes of HeLa cohesin purification buffer 3 (25 mM NaH_2PO_4/Na_2HPO_4, pH 7.5; 150 mM NaCl; 5% glycerol; 1 mM EDTA). Bound protein was eluted with 5 ml of HeLa cohesin purification buffer 3 supplemented with 0.5 mg/ml 3xFLAG peptide. Eluates were concentrated to approximately 0.2 ml using Vivaspin 6 100 kDa MWCO ultrafiltration units (Sartorius; VS0642), frozen in liquid nitrogen, and stored at -80°C.

S. cerevisiae condensin was expressed in and purified from *S. cerevisiae* as described previously.[2] Cell lysates were prepared in buffer A (50 mM TRIS-HCl, pH 7.5; 200 mM NaCl; 5% glycerol; 5 mM β-mercaptoethanol; 20 mM imidazole) supplemented with 1× cOmplete EDTA-free protease inhibitor mix (Roche; 11873580001) using a FreezerMill (Spex). The lysate was cleared by centrifugation and loaded onto a 5-mL HisTrap column (GE Healthcare), and eluted with 220 mM imidazole in buffer A. Eluate fractions were supplemented with 1 mM EDTA, 0.2 mM PMSF, and 0.01% Tween-20, incubated overnight with Strep-Tactin Superflow high capacity resin (IBA; 2-1208-010), and eluted with buffer B (50 mM TRIS-HCl, pH 7.5; 200 mM NaCl; 5% glycerol; 1 mM DTT) containing 10 mM desthiobiotin. The eluate was concentrated by ultrafiltration and further purified by size-exclusion chromatography using a Superose 6 column (Cytiva) pre-equilibrated in buffer B containing 1 mM $MgCl_2$. The purified protein was snap-frozen and stored at –80°C until use.

S. cerevisiae SMC5/6 and NSE5/6 was expressed, purified, and fluorescently labelled from *E.coli* as described previously.[9,38,65] *E. coli* cells were harvested by centrifugation and resuspended in 3–4 times the pellet volume of lysis buffer (50 mM Tris-HCl, pH 7.5; 300 mM NaCl; 5% glycerol; 25 mM Imidazole) freshly supplemented with 5 mM DTT, 1 mM PMSF, and 750 units of SM nuclease. All subsequent buffers, except the gel filtration buffer, contained 2 mM DTT. Cells were lysed by sonication on ice using a VS70T tip with a SonoPuls unit (Bandelin) at 40% output for 15 minutes with pulsing (1 s on / 1 s off), typically yielding a total energy output of 15 kJ. The lysate was clarified by centrifugation at 40,000 g for 30 minutes, and the supernatant was applied onto a 5 ml StrepTrap column (GE Healthcare). After washing with 10 column volumes (CV) of lysis buffer, the bound material was eluted with 4 CV of lysis buffer supplemented with 2.5 mM desthiobiotin, collecting fractions of 1.5 ml.

Fractions containing the complex were then applied onto a 5 ml HiTrap Heparin column (Cytiva). After washing with 5 CV of lysis buffer, the bound material was eluted with 4 CV of Heparin elution buffer (20 mM Tris, pH 7.5; 1,000 mM NaCl; 2 mM DTT). Fractions of 1.5 ml were collected, and those containing the target were concentrated using Amicon Ultra centrifugal filter units (50 kDa cutoff; Millipore). The protein was then injected onto a Superose6 10/300 GL size-exclusion chromatography (SEC) column. The standard SEC buffer contained 20 mM Tris-HCl, pH 7.5; 250 mM NaCl; 1 mM TCEP.

For purifying NSE5/6, lysates were prepared as described for SMC5/6, using the same lysis buffer, except that 5 mM DTT was replaced by 5 mM beta-mercaptoethanol. Fractions containing the complex at reasonable purity were loaded onto a 5 ml HiTrap Heparin column (Cytiva), and the bound protein was eluted with a gradient from buffer A to buffer B (20 mM Tris-HCl, pH 7.5; 1 M NaCl; 2 mM DTT). Fractions with sufficient purity were concentrated and injected onto a Superdex200 Increase 10/300 GL SEC column in a buffer containing 20 mM Tris, pH 7.5; 300 mM NaCl; 1 mM TCEP.

To reconstitute octameric complexes by size-exclusion chromatography, purified SMC5/6 hexamer and NSE5/6 were mixed in a total volume of 500 μl with a 1.5× molar excess of NSE5/6. This mixture was then subjected to SEC using Superose6 Increase 10/300GL.

S. cerevisiae SMC5/6 was expressed, purified, and fluorescently labelled from *S. cerevisiae* as described in Pradhan et al.[7] with small modifications. Cells were lysed using a Freezer Mill 6870 (SPEX). Proteins were extracted by adding one cell volume of

IPP150 buffer (50 mM Tris-HCl, pH 8.0; 150 mM NaCl; 10% glycerol; 0.1% IGEPAL CA-630; 1 mM DTT) with 10 mM MgCl2 and complete EDTA-free protease inhibitor (Roche Applied Science), followed by a 1-hour benzonase treatment (Merck) at 4°C. The cleared extracts were combined with IgG Sepharose FastFlow (Merck) and incubated for 2 hours at 4°C and washed with STO500 buffer (50 mM Tris-HCl pH 8.0, 500 mM NaCl, 2 mM $MgCl_2$, 0.5 mM tris(2-carboxyethyl)phosphine (TCEP), 10% glycerol, 0.1% IGEPAL CA-630) and eluted in 3 ml of STO500 containing TEV protease. The eluted fraction was diluted fourfold in CBB500 buffer (50 mM Tris-HCl, pH 8.0; 500 mM NaCl; 1 mM $Mg(CH_3COO)_2$; 1 mM imidazole; 2 mM $CaCl_2$; 1 mM DTT; 0.1% IGEPAL CA-630) supplemented with 1 M $CaCl_2$ and incubated with calmodulin Sepharose 4B (Merck) for 2 hours at 4°C. Following washes with CBB500 buffer, proteins were eluted using CEB500 buffer (50 mM Tris-HCl, pH 8.0; 500 mM NaCl; 1 mM $Mg(CH_3COO)_2$; 1 mM imidazole; 20 mM EGTA; 1 mM DTT; 0.1% IGEPAL CA-630). The eluate was concentrated using a Vivaspin20 ultrafiltration unit (100 KDa MWCO, Sartorius) with a simultaneous buffer exchange to STO500 buffer (50 mM Tris-HCl, pH 8.0; 500 mM NaCl; 2 mM $MgCl_2$; 0.5 mM TCEP; 10% glycerol; 0.1% IGEPAL CA-630).

NIPBL-ΔN was expressed and purified as described above[3,41] for NIPBL-MAU2 except that before elution from FLAG-M2 agarose, FLAG-M2 agarose beads were resuspended to one bead volume in 25 mM NaH_2PO_4/Na_2HPO_4 pH 7.5, 150 mM NaCl, 5 % glycerol, 50 mM imidazole pH 7.5 and split in half for fluorescent labelling with Atto550 and JF646 (see below).

Fluorescent labelling of SMC5/6 and estimation of the labelling efficiency

SMC5/6 hexamer purified from *E.coli* with a C-terminal HALO tag on NSE2 was incubated with a 2-fold molar excess of Janelia-Fluor646 HaloTag Ligand (Promega; 12 μM SMC5/6 hexamer + 24 μM label). After incubation for 1 h at 25°C, the reaction was stopped and excess label was removed using a Zeba Spin desalting column (Thermo Fisher) equilibrated in SEC buffer (20 mM Tris pH 7.5, 250 mM NaCl, 1 mM TCEP).

SMC5/6 purified from *E.coli* and JF646 concentrations were measured independently using absorption measurements at 280 nm for SMC5/6 and at 646 nm for JF646, yielding a fraction of 58 ± 11 % (N = 8 independent measurements) JF646 molecules per SMC5/6 hexamer. Fluorescence Correlation Spectroscopy (FCS) was performed on samples of 10 nM SMC5/6 hexamers in a buffer containing 40 mM Tris-HCl pH 7.5, 50 mM NaCl, 2.5 mM $MgCl_2$, 1 mM TCEP at room temperature. The resulting autocorrelation functions were well described by a fit with a single component, indicating that no free fluorophores were present.

SMC5/6 purified from yeast (roughly 1 μM concentration) was incubated with 20 μM of Alexa647-SNAP label overnight at 4°C in the presence of 1 mM DTT. The complex was then purified using a Zeba Spin column equilibrated in STO500 buffer. The labelling efficiency of SMC5/6 purified from yeast was estimated similarly and resulted in a labelling efficiency of 22 ± 2 % (N = 3 independent measurements).

Fluorescent labelling of NIPBL-ΔN

Janelia Fluor 646 SE (Tocris; 6148) was dissolved in dimethylformamide (DMF) at 20 mM. HaloTag Amine (O2) Ligand (Promega; P6711) was dissolved in dimethylformamide (DMF) at 50 mM. HaloTag Amine (O2) Ligand was added to JF646 SE in a 248.7 μl reaction in DMF while stirring and was then supplemented with 1.3 μl diisopropylethylamine (Sigma) (final concentrations: 7 mM JF646 SE, 2.3 mM HaloTag ligand, 31 mM diisopropylethylamine). Labelling reactions were incubated at room temperature for ~16 hours protected from light. The reaction mixture was diluted 10-fold in solvent A (5 % acetonitrile, 0.1 % formic acid) and purified in five successive reverse phase HPLC runs using an Ultimate 3000 (ThermoFisher Scientific) equipped with a Kinetex 5μ XB- C18 100A, 250 x 4.6mm column using the following gradient of solvents: A (5 % acetonitrile, 0.1 % formic acid), B (acetonitrile, 0.1 % formic acid); 0 – 100 % B in 30 min at a flow rate of 0.8 ml / min. Peak fractions were pooled, lyophilized, resuspended in DMSO, frozen in liquid nitrogen and stored at -80°C. Fractions were analysed by incubating with purified HaloTag protein for 15 min at room temperature followed by SDS-PAGE and excitation using a Bio-Rad ChemiDoc MP.

Atto550 NHS-ester (ATTO-TEC; AD 550-35) was dissolved in dimethylformamide (DMF) at 20 mM. HaloTag Amine (O2) Ligand was added to Atto550 NHS-ester in a 245 μl reaction in DMF while stirring and was then supplemented with 5 μl diisopropylethylamine (Sigma) (final concentrations: 25 mM Atto550 NHS-ester, 8.3 mM HaloTag ligand, 115 mM diisopropylethylamine). Labelling reactions were performed as for Janelia Fluor 646 SE, except that reaction mixture was diluted 10-fold in solvent A (40% acetonitrile, 0.1 % Trifluoroacetic acid) and reverse phase HPLC was performed using the following gradient of solvents: A (40% acetonitrile, 0.1 % Trifluoroacetic acid), B (acetonitrile, 0.1 % Trifluoroacetic acid); 0 – 100 % B in 30 min at a flow rate of 0.8 ml / min.

To label recombinant NIPBL-ΔN with Atto550-HaloTag Ligand and JF646-HaloTag Ligand, the purification was split in half. Each aliquot was supplemented with excess Atto550-HaloTag Ligand or JF646-HaloTag Ligand and incubated for 15 min at room temperature protected from light. Beads were washed extensively with recombinant cohesin purification buffer 3 and bound protein was eluted and concentrated as described for NIPBL-MAU2 in Davidson et al.[3] The resulting labelling efficiencies were measured analogous to SMC5/6 and yielded 86 ± 4 % for NIPBL-ΔN-A550 (N = 7) and 85 ± 5 % for NIPBL-ΔN-JF646 (N = 5).

Double-tethered DNA assay for single-molecule imaging of DNA loop extrusion

DNA loop extrusion experiments and imaging were performed essentially as described previously[2,15,69–71] with one round of pegylation with 5 mg/ml methoxy-PEG-N-hydroxysuccinimide (MW 3500, LaysanBio) and 0.05 mg/ml biotin-PEG-N-hydroxysuccinimide (MW 3400, LaysanBio) in 0.1 M $NaHCO_3$, 0.55 M K_2SO_4 buffer.[72] Subsequently, three more rounds of pegylation with $MS(PEG)_4$

(MW 333.33, Thermo Fisher) in the same buffer were applied. Slides and coverslips were incubated overnight at 4°C in the dark and then washed with ultrapure water and dried by a N_2 stream.

After assembly of flow chambers by sandwiching coverslip and drilled glass slide using double-sided tape and sealing the edges using epoxy glue, 0.5 mg/ml streptavidin was incubated for 1 min in loop extrusion buffer (see below) omitting glucose oxidase, intercalating dyes, ATP, and protein. The flow cell was then washed with 100 μl of the same buffer. End-biotinylated λ-DNA (48.5 kbp, Ganji et al.[2]) was then introduced at a flow speed to reach an end-to-end extension of about 6-7 μm (30% of the contour length). Unbound DNA was washed out with up to 200 μl buffer. The DNA was nicked, preventing a buildup of plectonemic supercoils during DNA loop extrusion.[69,73–75]

DNA Loop extrusion reactions by human cohesin were carried out in a buffer containing 40 mM Tris-HCl pH 7.5, 50 mM NaCl (unless otherwise denoted), 2.5 mM $MgCl_2$, 2.5% D-glucose, 2 mM Trolox, 10 nM catalase, 18.75 nM glucose oxidase, 100 nM SYTOX Orange, 0.5 mg/ml BSA, 1 mM DTT, 1 mM ATP with 10–100 pM cohesin (from *Sf9* insect cells) and the indicated concentration of NIPBL-MAU2 at 37°C (Figures 1, 2, 3A–3G, S1, S3, and S4). For experiments in which cohesin-JF646 was photobleached, glucose oxidase was omitted from the loop extrusion buffer (Figures S3G, S3H, and S3J). For experiments with differentially labelled NIPBL-ΔN, the buffer was adjusted to 25 mM NaCl and 25 nM SYTOX Green (Figures 3H–3M, S4, and S5). Part of the experiments were performed with cohesin purified from HeLa cells in which case 1 nM HeLa cohesin was used and part was performed with cohesin purified from *Sf9* cells. The two cohesin purifications behaved similarly and the results of these experiments were pooled.

DNA loop extrusion experiments with yeast condensin (Figures 1E, 2G, 2H, S1M, and S1N) were carried out in a buffer containing 40 mM Tris-HCl pH 7.5, 50 mM NaCl, 2.5 mM $MgCl_2$, 2.5% D-glucose, 2 mM Trolox, 10 nM catalase, 18.75 nM glucose oxidase, 100 nM SYTOX Orange, 0.5 mg/ml BSA, 1 mM DTT, 1 mM ATP with 1 nM cohesin at room temperature (22 °C).

DNA loop extrusion experiments with yeast SMC5/6 from *E.coli* (Figures 2I, 2J, S1M, and S2) were carried out in a buffer containing 40 mM Tris-HCl pH 7.5, 50 mM NaCl, 2.5 mM $MgCl_2$, 2.5% D-glucose, 2 mM Trolox, 10 nM catalase, 18.75 nM glucose oxidase, 100 nM SYTOX Orange, 0.5 mg/ml BSA, 1 mM TCEP, 1 mM ATP with 3 nM SMC5/6 hexamer at 30°C or in the same buffer but with 100 mM NaCl, 7.5 mM $MgCl_2$ as before.[9] DNA loop extrusion experiments with yeast SMC5/6 from yeast (Figures 1E and S2) were performed in the same buffer with 100 mM NaCl, 7.5 mM $MgCl_2$ as in Pradhan et al.[7] For experiments in which SMC5/6-JF646 was photobleached, glucose oxidase was omitted from the loop extrusion buffer (Figures S2F, S2G, S2I, and S2J).

All data were acquired using an exposure time of 100 ms per channel unless otherwise stated. For DNA loop extrusion without monitoring differentially labelled NIPBL-ΔN, the 561 nm-channel was used to image SYTOX Orange-stained DNA and the 640 nm-channel was used to alternatingly monitor the SMC complex. The effective time resolution in these experiments was thus 200 ms. For experiments with differentially labelled NIPBL-ΔN, the 480 nm channel was used to image SYTOX Green-stained DNA, the 561 nm channel was used to image NIPBL-ΔN-A550, and the 640 nm channel was used to image NIPBL-ΔN-JF646. The time resolution in these experiments was thus 300 ms. Experiments with the aim to visualize exchanges of NIPBL-MAU2 were performed with the N-terminal truncation of NIPBL, NIPBL-ΔN-A550 and NIPBL-ΔN-JF646, because NIPBL-MAU2 is prone to aggregation which is alleviated by NIPBL-ΔN during DNA loop extrusion experiments and was thus more suitable to image single NIPBL molecules.

To evaluate whether imaging at 200 ms time resolution potentially omits short phases of loop extrusion, diffusion, or slipping, experiments with human cohesin were also performed while imaging SYTOX Orange-stained DNA at 20 ms exposure time, yielding thus a 10-fold higher sampling rate compared to the remainder of the experiments.

Image series were acquired for 15 min after flush-in of SMC proteins.

Fluorescence Correlation Spectroscopy (FCS)

Fluorophore diffusion measurements were conducted using version 1 coverslips on a Picoquant Microtime 200 microscope, which was operated using Symphotime software at room temperature. To focus a 640 nm laser, a 60x Olympus UPSLAPO 60XW water immersion objective with a working distance of 280 μm and a numerical aperture of 1.2 was used. Prior to the experiment, the molecular brightness of a Alexa647 fluorophore solution was optimized by adjusting the correction collar of the objective. The emission light was subsequently directed through a 50 μm pinhole, split by a dichroic mirror, and filtered through a 600/75 optical band pass filter (Chroma, Bellow Falls). Fluorescence emission was collected by single-photon avalanche-diode detectors (PD5CTC and PD1CTC, Micro Photon Devices, Bolzano).

For fitting of the FCS curves, the size of the confocal volume was determined from measurements of the free Alexa647 by fitting a single-component diffusion model with triplet state (a diffusion constant of 297 $\mu m^2/s$ was used[76]). The axial and lateral sizes of the confocal volume were fixed for further analysis. FCS amplitudes and diffusion coefficients were subsequently fitted for curves recorded on SMC5/6-JF646 containing samples.

Protein complex structure prediction using AlphaFold2

AlphaFold2 predictions were generated using ColabFold, running on Google Colab[68] using the following parameters: msa_mode=mmseqs2_uniref_env; pair_mode=unpaired_paired; num_models=1 or 5 (predictions of large complexes quickly run out of GPU memory in which case only 1 model could be predicted); num_recycles=3; recycle_early_stop_tolerance=auto; max_msa=auto; num_seeds=1; use_dropout=True. The sequences used to generate the predictions are listed in Table S1. Protein structures were rendered using UCSF ChimeraX (Figures 6A–6C; Goddard et al.[77]).

QUANTIFICATION AND STATISTICAL ANALYSIS

Quantification and segmentation of kymographs

Images were cropped and processed by a median filter with window size 5 pixels (scipy.ndimage.median_filter (Virtanen et al.[78])) and background was subtracted using a Top-Hat filter of size 10 pixels (scipy.ndimage.white_tophat (Virtanen et al.[78])). Quantification of DNA loop size and position was performed as described previously.[15] In brief, the intensity of the loop is normalized to the intensity along the entire DNA molecule and multiplied by the known length of the DNA molecule (48.5 kbp). The loop position was determined as the relative position of the loop from one randomly selected end of the DNA for each molecule but kept constant for all analyses. Half of the loop size at every moment was added to this position. The reported loop position (in kbp) refers thus to the tip of the extruded loop. DNA loop size and position were plotted concomitantly versus time (Figure 1B) and in a two-dimensional plot (Figures S1C and S1D). Segmentation of the kymographs into phases of loop extrusion, loop diffusion, and loop slipping was performed under assistance of a change point detection algorithm. We found that an entirely automatic segmentation was not robust and returned spurious results on some traces or on parts of traces. Therefore, we subsequently manually curated the automatic segmentation (Figure S1A). Change point detection was performed as follows. Traces of loop size over time were first filtered using a Savitzky–Golay filter with window length of 5 seconds and order 1 (implemented as part of the *scipy* package[78]; also shown in Figures throughout the manuscript). Change point detection was performed using a window-based change point detection algorithm, implemented in the *ruptures* package[79] (function *ruptures.Window*), with a window length of 10 seconds and an autoregressive model as cost function with order 2. The number of potential change points was not restricted. This procedure generally returned too many change points which were subsequently merged as follows (illustrated in Figure S1A). Following the error estimation previously presented in Davidson et al.[15] (Extended Data Figure 10 and Supplementary Information), we estimated the error associated with the loop size measurement (in the order of 4-10% at an end-to-end length of 20% of the contour length; Figure S1B). The loop size over time in every segment in between two automatically found change points was subject to a linear regression. If the difference in loop size within the segment is less than the associated error in loop size determination, given the median measured loop size in the segment, the segment was labelled as diffusion phase. If the change in loop size exceeded the associated loop size uncertainty, the segment was labelled as extrusion phase if the slope of the loop size over time within the segment was positive, and the segment was labelled as slipping phase otherwise. Phases in which loops colocalize with the DNA ends (5% of the DNA length at each side) were labelled as 'stalled' and excluded from further analysis. Neighbouring segments are subsequently merged if they were assigned the same label. As illustrated in Figure S1A, this procedure was not entirely robust on some parts of traces for which we subsequently curated the segmentation manually. After manual curation, the change in loop position was evaluated again as described above to assign each segment one of the labels 'diffusion', 'extrusion', or 'slipping'. Afterwards, loop extrusion and slipping phases were manually divided into smaller segments if the traveling direction of the loop changed during the extrusion/slipping phase, representing the last stage of segmentation and classification. The direction of each extrusion and slipping phase was subsequently annotated by subjecting the loop position over time within each segment to a linear regression and classifying the segment as direction_1/direction_2 based on the slope of the linear fit. Note that the nomenclature of the direction is arbitrary. Here, the first direction to which the loop travels is called direction_1.

To determine whether loop extrusion phases proceed asymmetrically or symmetrically, the amount of DNA towards both sides (L_{dir1} and L_{dir2} in Figures 2 and S3) were quantified by dividing the relative fluorescence of both DNA segments to the left and right of the loop by the length of the DNA molecule (48.5 kbp), as was done previously.[2,5,7] The ratio $\Delta L_{dir1} / \Delta L_{dir2}$ was computed across the duration of the annotated loop extrusion phase.

DNA loop extrusion traces by human cohesin were usually acquired at a time resolution of 200 ms (100 ms exposure time for the DNA and cohesin-JF646 channel, respectively, in the absence of labelled NIPBL-ΔN). To check whether phases of loop extrusion, diffusion, or slipping exist which are too short to be segmented with a time resolution of 200 ms, cohesin-mediated DNA loop extrusion traces were also acquired at a time resolution of 20 ms (only the DNA channel was imaged). This data set was then segmented and classified using the time resolution of 20 ms. Additionally, the same data set was subsampled by averaging 5 subsequent frames of the DNA channel (thus effectively increasing the exposure time to 100 ms) and omitting the following 5 frames (thus mimicking the imaging of cohesin-JF646 for another 100 ms). The subsampled data set was segmented and classified independently. The segmentation results of both data sets were quantitatively compared to check for short phases in the 20 ms data set which were missed in the subsampled data set (Figures S1E–S1H). 76 ± 17 % (probability and 95% binomial confidence interval) of all traces were segmented into an equal number of phases (Figure S1E; Jaccard index of 0.80 [N_{union} = 184, $N_{intersection}$ = 148]) and the change points were set, on average, at the same time (mean time difference 0.14 s; Figure S1F) with low variation between individual change points (SD = 1 s; Figure S1F). The fraction of uni- vs. bidirectional traces was identical (Figure S1G) and there was no significant change between the duration of loop extrusion, diffusion, and slipping phases (Figure S1H). We conclude that a time resolution of 200 ms is sufficient to segment traces of DNA loop extrusion into phases of loop extrusion, diffusion, and slipping and that no significantly shorter phases exist.

Quantification of DNA loop extrusion, loop diffusion, and loop slipping kinetics

The following metrics were calculated which characterize DNA loop extrusion traces of all eukaryotic SMC complexes: loop extrusion rate, loop slipping rate, diffusion constant, loop lifetime, the fraction of unidirectional traces, frequency of direction switches, and the fraction of diffusing and slipping loops.

The loop extrusion (Figures S1N and S2E) and loop slipping rate (Figure S5I) were determined *via* a linear fit to the loop size across the loop extrusion or loop slipping phase, respectively. To quantify the diffusion constant of loops during diffusion phases (Figure S5H), the mean squared displacement (MSD) of the loop during the diffusion phase was calculated. The diffusion constant was subsequently determined *via* linear regression of the form $MSD(\tau) = D\tau + o$ (diffusion constant D, time lag τ, and offset o due to finite localization uncertainty) to the first 10% of the available time lags for sufficient data points of the fit and to avoid flattening of the MSD curve when the loop reaches the DNA ends.

The loop lifetime (Figures 3C and S4F) was determined as the interval from the beginning of the first loop extrusion phase until the complete dissociation of the loop. In cases in which acquisition was stopped before loop dissociation, the loop lifetime was computed from the beginning of loop extrusion until the end of acquisition.

A trace was labelled as extruding toward one direction only (unidirectional; Figures 1E, 3A, and S4A) if a trace showed at least two extrusion phases in only one direction and no extrusion phase in the other direction. A trace was labelled as extruding bidirectionally if the trace exhibited at least one extrusion phase in each direction. Traces which exhibited only one extrusion phase were not considered because it is unclear whether the SMC complex could only undergo a single phase of extrusion despite being a bidirectional extruder or whether the SMC complex was indeed a unidirectional extruder. The average frequency of direction switches was computed for each loop by dividing the number of direction switches per trace by the loop lifetime (Figures 3B and S4B) for traces which showed at least one direction switch.

The fraction of traces which showed loop diffusion (Figure S3E) and loop slipping (Figure S3F) was computed as the fraction of traces with at least one diffusion or slipping phase, respectively.

Bleaching and annotation of NIPBL-ΔN presence

The intensity of cohesin-JF646 (in bleaching experiments; Figures S3G, S3H, and S3J), SMC5/6 (Figure S2), and NIPBL-ΔN-A550/JF646 was computed as the average intensity in the respective channel at the loop position over a window of 5 pixels around the loop centroid position. Background was subtracted by averaging the intensity in a selected region adjacent to the cropped DNA molecule in which no fluorescently labelled molecules bound unspecifically to the surface during the loop lifetime. The number of bleaching steps was determined by plotting the fluorescence intensity at the loop over time and counting the number of step-wise decreases to the background level, aided by a hidden Markov model (HMM) analysis[80] (e.g. Figure S3J). Only SMC complexes associated with a DNA loop were considered (which allows an assignment of the number of cohesin-JF646 bleaching steps to traces showing uni- (Figure S3G) or bidirectional extrusion (Figure S3H)). The appearance and disappearance (in the presence of the oxygen-scavenging system) or bleaching (in the absence of the oxygen-scavenging system) of NIPBL-ΔN-A550/JF646 (Figures 3H–3M and S5B–S5I) was assessed analogously.

To assess whether bidirectionally extruding SMC5/6 complexes are potentially dimers that appear to be monomers given the imperfect (<100%) labelling efficiency, we compared the potential fraction of SMC5/6 dimers to the fraction of bidirectionally extruding SMC5/6 complexes as follows. Given the labeling efficiency p_{label}, the probability that an unlabeled SMC5/6 dimer was observed to extrude a DNA loop is $(1- p_{label})$.[2] Similarly, when a single fluorophore was observed at the stem of the loop, the probability that an SMC5/6 dimer extruded the loop is $1- p_{label}$ and the probability that a SMC5/6 dimer extrudes a DNA loop when two fluorophores were observed is 1. We denote the number of observed loops with 0, 1, and 2 fluorophores N_0, N_1, and N_2, respectively. The expected number of SMC5/6 dimers, given the labeling efficiency p_{label}, is thus $N_{potential\ dimers} = N_0(1- p_{label})^2 + N_1(1- p_{label}) + N_2$ and the fraction of potential dimers, given the observed set of bleaching traces N, is $N_{potential\ dimers}/N$. We then compare the quantity $N_{potential\ dimers}/N$ to the fraction of bidirectionally extruding SMC5/6 complexes (Figure S2K).

Testing the Markov property

Let us denote the state *k* of cohesin as being in an extrusion, diffusion, or slipping phase. A finite, first-order, discrete Markov chain is a stochastic process in which the probability to transition from state *k* to state *l* depends only on the current state (state *k*) but on states at previous points in time[81]: $P\{X(t+1) = l \,|\, X(0) = k_0, \ldots, X(t-1) = k_{t-1}, X(t) = k\} = P\{X(t+1) = l \,|\, X(t) = k\} = p_{kl}$. The Markov chain is thus determined by the transition matrix Π which summarizes all 3x3 possible transitions (here we consider three possible states):

$$\Pi = \begin{bmatrix} p_{11} & p_{12} & p_{13} \\ p_{21} & p_{22} & p_{23} \\ p_{31} & p_{32} & p_{33} \end{bmatrix}$$

$$p_{kl} \geq 0$$

$$p_{kk} = 0$$

$$\sum_{l=1}^{3} p_{kl} = 1$$

The transition probability p_{kl} is computed as the number of transitions from state k to state l, N, divided by the number of transitions from state k to any state, i.e. $p_{kl} = N_{kl} / \sum_{l} N_{kl}$.

Alternatively, the stochastic process might have memory, in which case the transition probability from state k (at time t) to state l (at time t+1) depends also on the previous state j (at time t-1), i.e. $p_{jkl} = P\{X(t+1) = l | X(t) = k, X(t-1) = j, \}$. A three-state transition matrix is constructed analogously to the two-state transition matrix Π. The chi-square statistic is subsequently used to test whether the Markov chain is a first order (memory-less, the null hypothesis H_0) or second order (with memory, H_1) process.[82] The chi-square statistic for the null hypothesis of state k (in other words: the hypothesis that the transition from the current state k to the future state l is independent of the past state j) is:

$$Q_k = \sum_{jl} N_{jk} \left(p_{jkl} - p_{kl}\right)^2 / p_{kl}$$

Where $p_{kl} = \sum_{j=0}^{3} N_{jkl} / \sum_{j=0}^{3} \sum_{m=0}^{3} N_{jkm}$ and $N_{jk} = \sum_{l} N_{jkl}$. If H_0 is true, Q_k has a chi-square distribution with $(3\text{-}1)^2$ degrees of freedom. Similarly, the joint hypothesis that the transition from all states is memory-less, i.e. that $p_{jkl} = p_{kl}\ \forall j,k,l = 0,1,2$, can be computed via the sum $Q = \sum_{k} Q_k$ which has a chi-square distribution with $3(2\text{-}1)^2$ degrees of freedom. The null hypothesis H_0 is rejected if the test result $P(X > Q_k)$ is significant at the significance level of $\alpha = 0.05$. The p-values for the three states are all > 0.05 across all conditions (Figure S3D), thus cohesin switches from one state to another without memory of the past state.

3D polymer simulations

3D polymer simulations were performed as described by Banigan et al.,[44] with small modifications. A genomic region comprising 5600 monomers (1 monomer = 2 kb) was simulated containing 8 repeating elements of TADs spanning 400, 100, and 200 monomers respectively. These 8 elements were averaged to generate the contact maps shown in Figure 4A. For switching loop extruders, the extruding side was switched according to the experimentally observed switching rate (Figure 3B). When loop diffusion and slipping were included, extruders spawned in the extruding state were changed into a diffusing or slipping state with a probability of 20% and 80%, respectively (Figure S1L) at a rate according to the experimentally observed lifetime of extruding phases (Figure 1D). When extruders were in a diffusing state, they changed into an extruding or slipping state with a probability of 50% (Figure S1L) at a rate according to the experimentally observed lifetime of diffusion phases (Figure 1D). Finally, when extruders were in a slipping state, they changed into a diffusing or extruding state with a probability of 80% and 20%, respectively (Figure S1L) at a rate according to the experimentally observed lifetime of slipping phases (Figure 1D). The time steps of the simulation and state-change rates were adjusted accordingly to let extruders extrude/diffuse/slip by 1 monomer per time step using the processivity and separation of loop extruders of 200 kb as in Banigan et al.[44] 1D simulations were equilibrated and 3D polymer simulations were subsequently performed as before.[44] From the resulting polymer configurations, contact maps were computed from 4000 conformations using the *contactmaps* module of the *openmmlib* package (https://github.com/mirnylab/openmm-polymer-legacy) with a contact radius of 5 monomers. Due to the sampling of the polymer dynamics in order to generate contact maps, the code was run on a node with access to a NVIDIA Tesla V100S using DelftBlue DHPC.[83]

CellPress
OPEN ACCESS

Supplemental figures

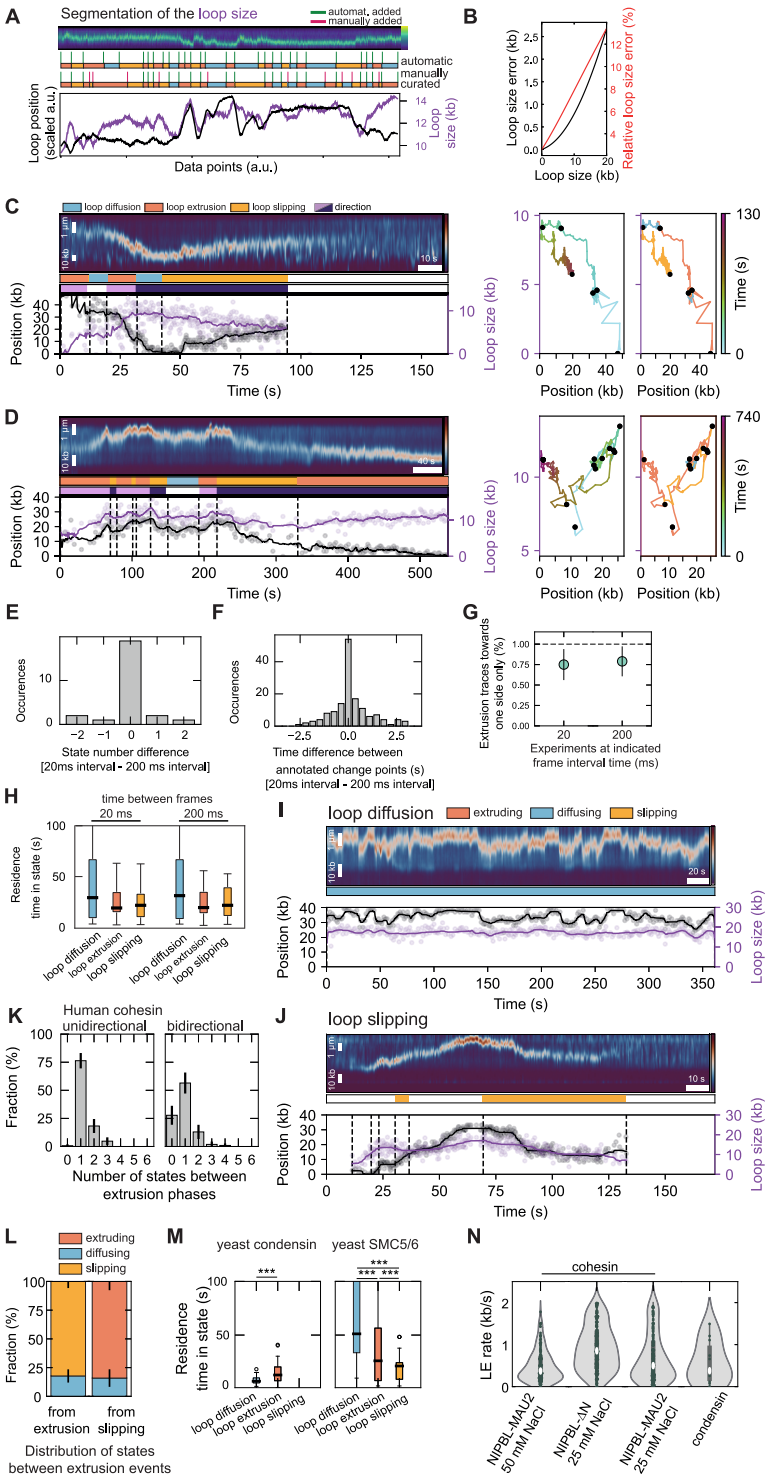

(legend on next page)

Figure S1. Comparison of DNA loop extrusion trace segmentation between data acquisition with 20 and 200 ms time resolution, related to Figures 1, 2, and 3.

Loop diffusion and slipping examples, state residence times for yeast SMC5/6 and yeast condensin.

(A) Example kymograph and quantified loop position and size of cohesin-mediated DNA loop extrusion (NIPBL-MAU2:cohesin ratio 2; 50 mM NaCl). The result of the automatic segmentation (STAR Methods) as well as the manually curated segmentation of the loop size over time is annotated.

(B) The (relative) loop size error increases with increasing loop size (DNA length 48.5 kbp, end-to-end length 3.5 μm [20% of the contour length]).

(C) Example kymograph of cohesin-mediated DNA loop extrusion (left; NIPBL-MAU2:cohesin ratio 2; 50 mM NaCl). Loop position and size are quantified and segmented into loop extrusion, diffusion, and slipping phases. The two panels on the right display a two-dimensional plot of the loop size versus loop position. Black dots demarcate boundaries between diffusion, extrusion, and slipping phases. Diffusion phases move on horizontal lines in this graph, and extrusion and slipping phases are demarcated by diagonal lines. Dots represent raw data, solid lines represent a smoothed version using a Savitzky-Golay filter with window length of 5 s and order 1 (STAR Methods).

(D) As (C) but for a loop extrusion trace in which extrusion phases in both directions are present as shown in Figure 1B (NIPBL-MAU2:cohesin ratio 12; 50 mM NaCl).

(E) Difference in the number of phases (segments) between the dataset acquired at 20 ms frame interval time and the subsampled one (interval time 200 ms). Negative values indicate that fewer segments were segmented in the 20-ms interval dataset than in the 200-ms dataset (NIPBL-MAU2:cohesin ratio 2; 50 mM NaCl).

(F) Time between the annotated change points (time points between segments) in the dataset with an interval time of 20 and 200 ms between frames. 74% of all change points coincide between the two annotations within 1 s (N = 147 segments; NIPBL-MAU2:cohesin ratio 2; 50 mM NaCl). Negative values indicate that the change point in the 20-ms interval dataset was annotated prior to the respective change point in the 200-ms dataset.

(G) Fraction of traces with at least two extrusion events that displayed only unidirectional extrusion (N = 25 traces each; NIPBL-MAU2:cohesin ratio 2; 50 mM NaCl). Error bars denote the binomial 95% confidence interval.

(H) Duration of diffusion, extrusion, and slipping phases in the annotated datasets acquired at 20 ms frame interval time and the subsampled one (interval time 200 ms; NIPBL-MAU2:cohesin ratio 2; 50 mM NaCl). Black horizontal lines are median values, the box extends between the first and third quartile, and the whiskers extend to 1.5 × IQR. No statistically significant difference was found between loop diffusion, extrusion, and slipping states between the two datasets. Statistical significance was assessed by a Mann-Whitney test with Bonferroni correction (p values are 0.9514, 0.6504, and 0.4710 for loop diffusion, extrusion, and slipping states, respectively).

(I) Example kymograph of human cohesin showing loop diffusion (NIPBL-MAU2:cohesin ratio 2; 50 mM NaCl) as in (C).

(J) Example kymograph of human cohesin showing loop slipping (NIPBL-MAU2:cohesin ratio 2; 50 mM NaCl) as in (C).

(K) Number of intervening states between extrusion events for traces (pooled from NIPBL-\bidirectional extrusion (N = 108). Bar height denotes the probability of finding the annotated number of steps between extrusion events. Error bars denote the binomial 95% confidence interval. Unidirectional extruders always have at least one intervening phase (diffusion or slipping phase) between extrusion phases, while bidirectional extruders may also switch extrusion direction without a noticeable intervening diffusion or slipping phase. However, subsequent extrusion phases were most commonly interleaved by one or two diffusion or slipping phases.

(L) Distribution of states between direction switches in extrusion (N = 90) and slipping (N = 88) events (pooled from NIPBL-MAU2:cohesin ratios 0.1, 1, 2, and 12; 50 mM NaCl). Error bars denote the binomial 95% confidence interval. Cohesin in an extrusion phase transitioned most often into a slipping phase and vice versa, i.e., cohesin transitioned most of the time between loop extrusion and slipping phases.

(M) Duration of diffusion, extrusion, and slipping states for yeast condensin (N = 16, 48, and 1, respectively) and yeast SMC5/6 (N = 52, 124, and 80, respectively; purification from *E. coli*; 100 mM NaCl, 7.5 mM $MgCl_2$). Black horizontal lines are median values, the box extends between the first and third quartile, and whiskers extend to 1.5 × IQR. Statistical significance was assessed by a Mann-Whitney test with Bonferroni correction (***$p < 0.001$).

(N) DNA loop extrusion rate of human cohesin with the annotated version of NIPBL in a buffer containing the indicated concentration of NaCl and of yeast condensin in 50 mM NaCl. The white dot marks the median value (N = 180, 241, 240, and 11, from left to right), the box extends to the quartiles, and the whiskers denote the interquartile range.

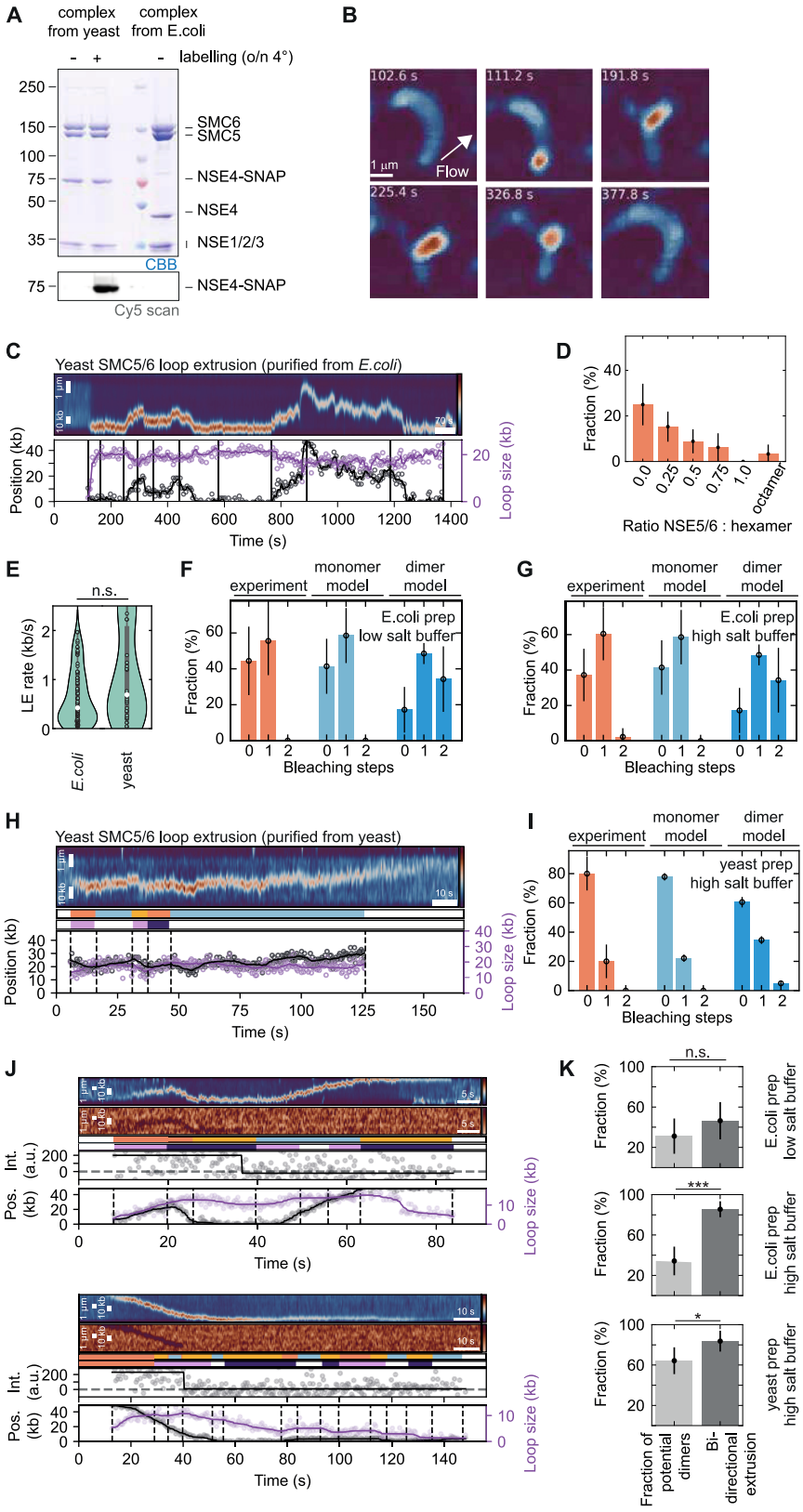

(legend on next page)

Figure S2. DNA loop extrusion by single SMC5/6 hexamers, related to Figure 1

(A) Detection of SMC5/6 hexamer subunits by SDS-PAGE and Coomassie staining for the unlabeled (1st lane), NSE4-Alexa647-labeled (2nd lane) SMC5/6 complex purified from yeast cells, and for the unlabeled SMC5/6 purified from *E. coli* as in Taschner and Gruber.[38]

(B) Fluorescence imaging snapshots showing DNA loop extrusion by an SMC5/6 hexamer purified from *E. coli* during side flow (100 mM NaCl, 7.5 mM $MgCl_2$).

(C) Example kymograph of DNA loop extrusion by an SMC5/6 hexamer purified from *E. coli* (50 mM NaCl, 2.5 mM $MgCl_2$). Dots represent raw data, solid lines represent a smoothed version using a Savitzky-Golay filter with window length of 5 s and order 1 (STAR Methods).

(D) Loop extrusion efficiency with varying ratios of NSE5/6 to the SMC5/6 hexamer purified from *E. coli*. No loop extrusion is observed at an equimolar ratio of NSE5/6 and the SMC5/6 hexamer. A co-purification of NSE5/6-bound SMC5/6 hexamer (octamer) shows a small fraction of loop extrusion, potentially due to dissociation of NSE5/6 from the SMC5/6 hexamer that allows loop extrusion. Bar heights denote the probability of finding a DNA with a loop and the error bar denotes the binomial 95% confidence interval (N = 92, 124, 124, 64, 74, and 84 DNA molecules, from left to right; 50 mM NaCl, 2.5 mM $MgCl_2$).

(E) DNA loop extrusion rate of the SMC5/6 hexamer, purified from *E. coli* (Taschner and Grube[38]) and from yeast (100 mM NaCl, 7.5 mM $MgCl_2$). The white dot marks the median value (0.4 ± 0.5, median ± SD, N = 83 for *E. coli*; 0.7 ± 0.9, median ± SD, N = 30 for *E. coli*), the box extends to the quartiles, and the whiskers denote the interquartile range. Statistical significance was assessed by a two-sided Kolmogorov-Smirnoff test (p = 0.087).

(F) Bleaching step distribution of JF646-labeled SMC5/6 hexamers purified from *E. coli* in 50 mM NaCl, 2.5 mM $MgCl_2$ with a labeling efficiency of 58% ± 11% (N = 27 for the experiment; N = 1,000 simulated monomer/dimer complexes). The monomer model fits the experimental data while the dimer model does not. Error bars denote the 95% binomial confidence interval for experimental data and the range of the predicted monomer/dimer bleaching step distributions for a labeling efficiency of 47% (lower end) and 69% (upper end).

(G) As for (F) but in a 100 mM NaCl, 7.5 mM $MgCl_2$ buffer (N = 27 for the experiment; N = 1,000 simulated monomer/dimer complexes), which is the buffer in which dimers of SMC5/6 hexamers were reported to extrude by Pradhan et al.[7]

(H) Example kymograph of DNA loop extrusion by an SMC5/6 hexamer purified from yeast (100 mM NaCl, 7.5 mM $MgCl_2$) as in (C).

(I) As for (G) but for SMC5/6 purified from yeast with a labeling efficiency of 22% ± 2% (N = 50 for the experiment; N = 1,000 simulated monomer/dimer complexes) in a 100-mM NaCl, 7.5-mM $MgCl_2$ buffer in which dimers of SMC5/6 hexamers were reported to extrude by Pradhan et al.[7] Error bars denote the 95% binomial confidence interval for experimental data and the range of the predicted monomer/dimer bleaching step distributions for a labeling efficiency of 20% (lower end) and 24% (upper end).

(J) Example kymographs of DNA loop extrusion by JF646-labeled yeast SMC5/6 purified from *E. coli* (top) and yeast (bottom) in a 100 mM NaCl, 7.5 mM $MgCl_2$ buffer as in (C). The JF646-labeled SMC5/6 molecules were bleached and the background-subtracted fluorescence intensity is shown simultaneously with the quantified loop size and position over time. Step finding (black line) in intensity traces was performed using *sfHMM*[80] using default parameters and *psf = 0.0001*.

(K) Analysis of the potential fraction of SMC5/6 dimers estimated from the labeling efficiency compared with the observed fraction of bidirectional extrusion. Error bars denote the 95% binomial confidence interval. Statistical significance was assessed using Fisher's exact test (n.s. $p > 0.05$; $^*p \leq 0.05$; $^{***}p < 0.001$). For experiments in 100 mM NaCl and 7.5 $MgCl_2$, the fraction of potential dimers cannot account for the fraction of complexes observed to extrude bidirectionally.

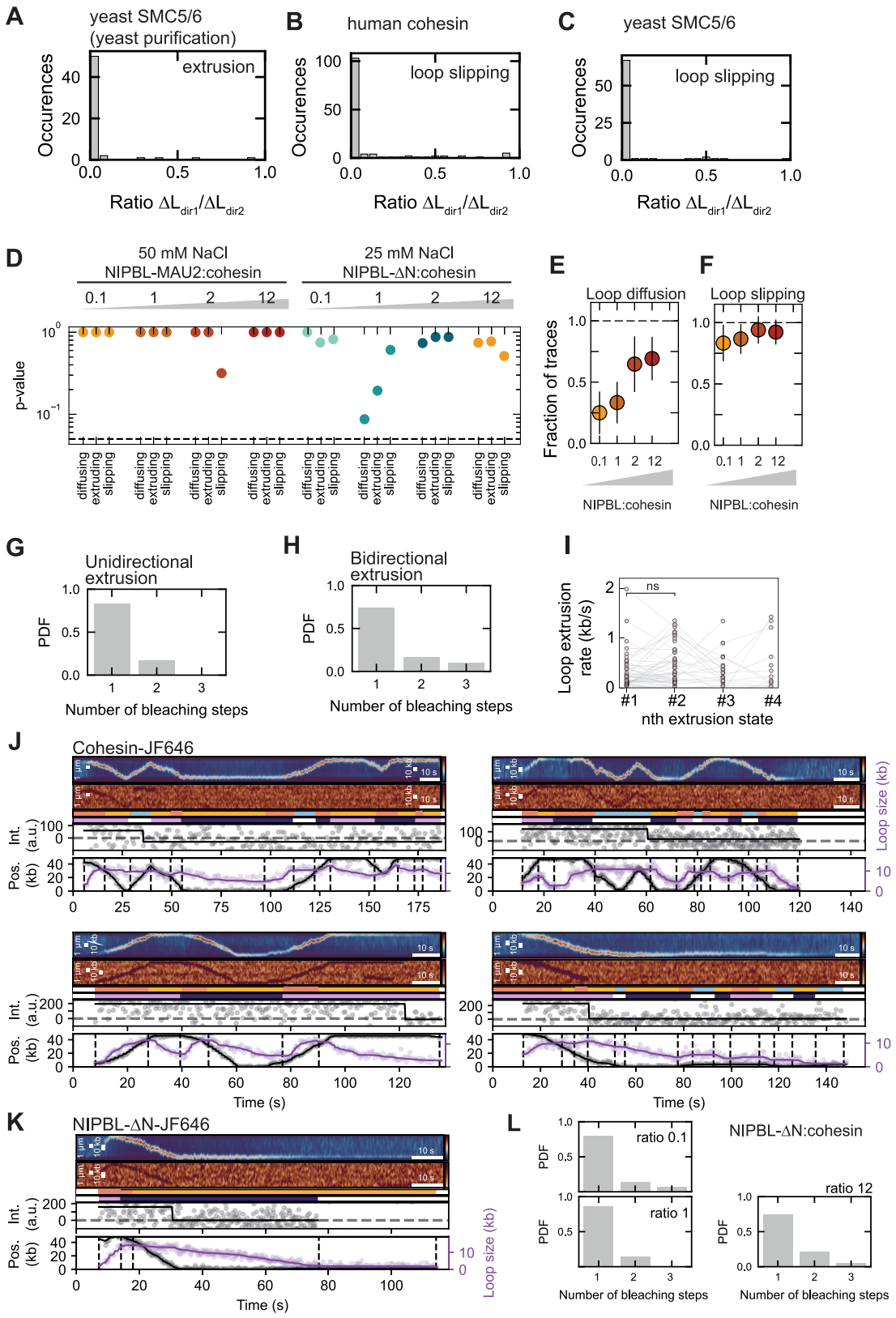

(legend on next page)

Figure S3. Loop slipping is, like extrusion, asymmetric, related to Figures 1, 2, and 3

The sequence of loop diffusion, extrusion, and slipping events is a Markov chain and the excess of NIPBL-MAU2 and STAG1 over cohesin modulate the occurrence of diffusion and slipping phases. Bidirectional extrusion is the result of monomeric cohesin complexes.

(A) Distribution of the ratio $\Delta L_{dir1}/\Delta L_{dir2}$ for extrusion events of yeast SMC5/6 purified from yeast cells (N = 56 events; 100 mM NaCl, 7.5 mM $MgCl_2$). Yeast SMC5/6 purified from yeast cells exhibits asymmetric extrusion phases (93% ± 7% [mean ± 95% binomial confidence interval] of $\Delta L_{dir1}/\Delta L_{dir2}$ values below 0.1).

(B) Distribution of the ratio $\Delta L_{dir1}/\Delta L_{dir2}$ for slipping events of human cohesin (N = 130 events; pooled from NIPBL-MAU2:cohesin ratios 0.1, 1, 2, and 12; 50 mM NaCl).

(C) Distribution of the ratio $\Delta L_{dir1}/\Delta L_{dir2}$ for slipping events of yeast SMC5/6, purified from *E. coli* (N = 77 events; 100 mM NaCl, 7.5 mM $MgCl_2$).

(D) p value of the Markov property test for transitions starting from a loop diffusion, extrusion, and slipping state for all tested NaCl concentrations and NIPBL-MAU2:cohesin ratios. A value below 0.05 (dashed line indicates the violation of the Markov property and would suggest a system with memory).

(E) Fraction of diffusing cohesin complexes for varying ratios of NIPBL-MAU2:cohesin (50 mM NaCl; N = 24, 30, 17, and 26, from left to right). Dots denote the fraction, error bars denote the binomial 95% confidence interval.

(F) As for (B) but for loop slipping. Number of data points as in (B).

(G) Number of bleaching steps of human cohesin-JF646 for complexes that extrude unidirectionally (N = 169; pooled from NIPBL-MAU2:cohesin and NIPBL-ΔN:cohesin ratios 0.1, 1, 2, and 12; at 25 and 50 mM NaCl).

(H) Number of bleaching steps of human cohesin-JF646 for complexes that extrude bidirectionally (N = 62; pooled from NIPBL-MAU2:cohesin and NIPBL-ΔN:cohesin ratios 0.1, 1, 2, and 12; at 25 and 50 mM NaCl).

(I) Loop extrusion rate for the n^{th} extrusion state within single kymographs (N = 48, 48, 32, and 13, from left to right; pooled from NIPBL-MAU2:cohesin ratios 0.1, 1, 2, and 12; 50 mM NaCl).

(J) Example kymographs of DNA loop extrusion by JF646-labeled human cohesin in a 50 mM NaCl, 2.5 mM $MgCl_2$ buffer. Dots represent raw data, solid lines represent a smoothed version using a Savitzky-Golay filter with window length of 5 s and order 1 (STAR Methods). The JF646-labeled cohesin molecules were bleached and the background-subtracted fluorescence intensity is shown simultaneously with the quantified loop size and position over time. Step finding (black line) in intensity traces was performed using *sfHMM*[80] using default parameters and *psf* = *0.0001*.

(K) Example kymographs of DNA loop extrusion with a JF646-labeled NIPBL-ΔN in a 25 mM NaCl, 2.5 mM $MgCl_2$ buffer, as in (J).

(L) Number of bleaching steps of NIPBL-ΔN-A550/JF646 at increasing ratios of NIPBL-ΔN to cohesin in 25 mM NaCl (N = 43, 29, and 14, from top to bottom). NIPBL-ΔN-A550 and NIPBL-ΔN-JF646 were imaged in separate experiments to avoid potential colocalization of NIPBL-ΔN in different colors. The bleaching step distributions of NIPBL-ΔN-A550 and NIPBL-ΔN-JF646 were similar and subsequently pooled.

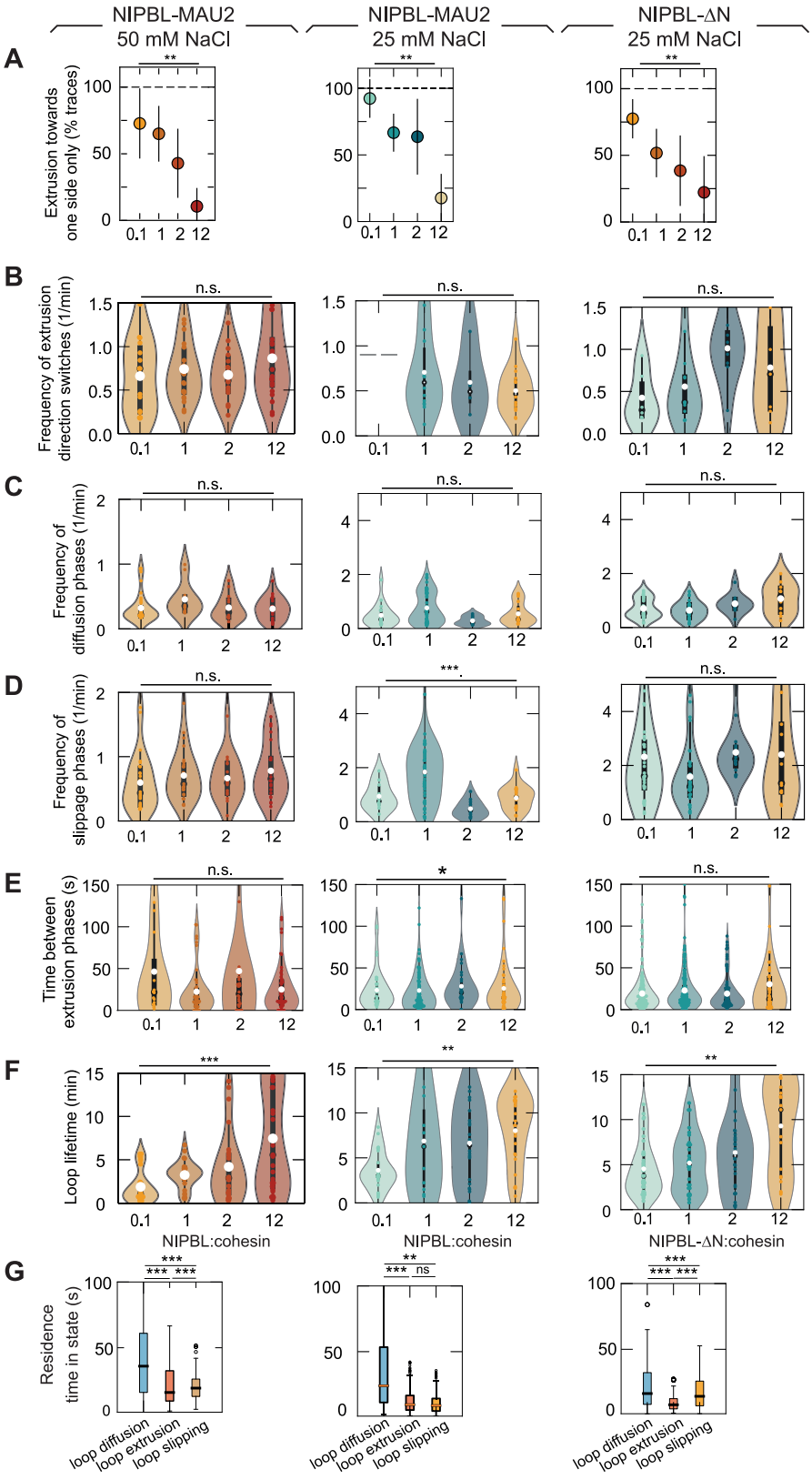

(legend on next page)

Figure S4. Dynamics of cohesin-mediated DNA loop extrusion in response to changing ionic strength conditions and NIPBL-ΔN, related to Figures 1 and 3

(A) Fraction of cohesin complexes undergoing at least two extrusion events that displayed only unidirectional extrusion (*N* = 41, 30, 17, 26; 13, 42, 11, 21; 31, 29, 13, and 9, from left to right). Error bars denote the binomial 95% confidence interval. Statistical significance was assessed by a chi-squared test.

(B) Frequency of extrusion direction switches (*N* = 41, 30, 17, 26; 1, 14, 4, 14; 6, 13, 8, and 7). The white dot denotes the mean. The box shows the quartiles of the dataset and the whiskers extend to 1.5 × IQR. Statistical significance was assessed by a Kruskal-Wallis test.

(C) Frequency of diffusion phases (*N* = 44, 12, 14, 20; 17, 53, 8, 16; 27, 25, 10, and 10). The white dot denotes the mean. The box shows the quartiles of the dataset and the whiskers extend to 1.5 × IQR. Statistical significance was assessed by a Kruskal-Wallis test.

(D) Frequency of slipping phases (*N* = 26, 25, 15, 22; 10, 44, 11, 16; 35, 33, 16, and 13). The white dot denotes the mean. The box shows the quartiles of the dataset and the whiskers extend to 1.5 × IQR. Statistical significance was assessed by a Kruskal-Wallis test.

(E) Time between subsequent extrusion phases (*N* = 16, 51, 30, 56; 39, 125, 27, 47; 221, 217, 111, and 59). The white dot denotes the mean. The box shows the quartiles of the dataset and the whiskers extend to 1.5 × IQR. Statistical significance was assessed by a Kruskal-Wallis test.

(F) Loop lifetime between the first extrusion event and loop disruption (*N* = 41, 31, 25, 37; 25, 11, 22, 26; 37, 30, 32, and 21). The white dot denotes the mean. The box shows the quartiles of the dataset and the whiskers extend to 1.5 × IQR. Statistical significance was assessed by a Kruskal-Wallis test.

(G) Duration of diffusion, extrusion, and slipping states (*N* = 93, 344, 257; 130, 294, 234; 390, 753, and 712). Black horizontal lines are median values, the box extends between the first and third quartile, and the whiskers extend to 1.5 × IQR. Statistical significance was assessed by a Mann-Whitney test with Bonferroni correction.

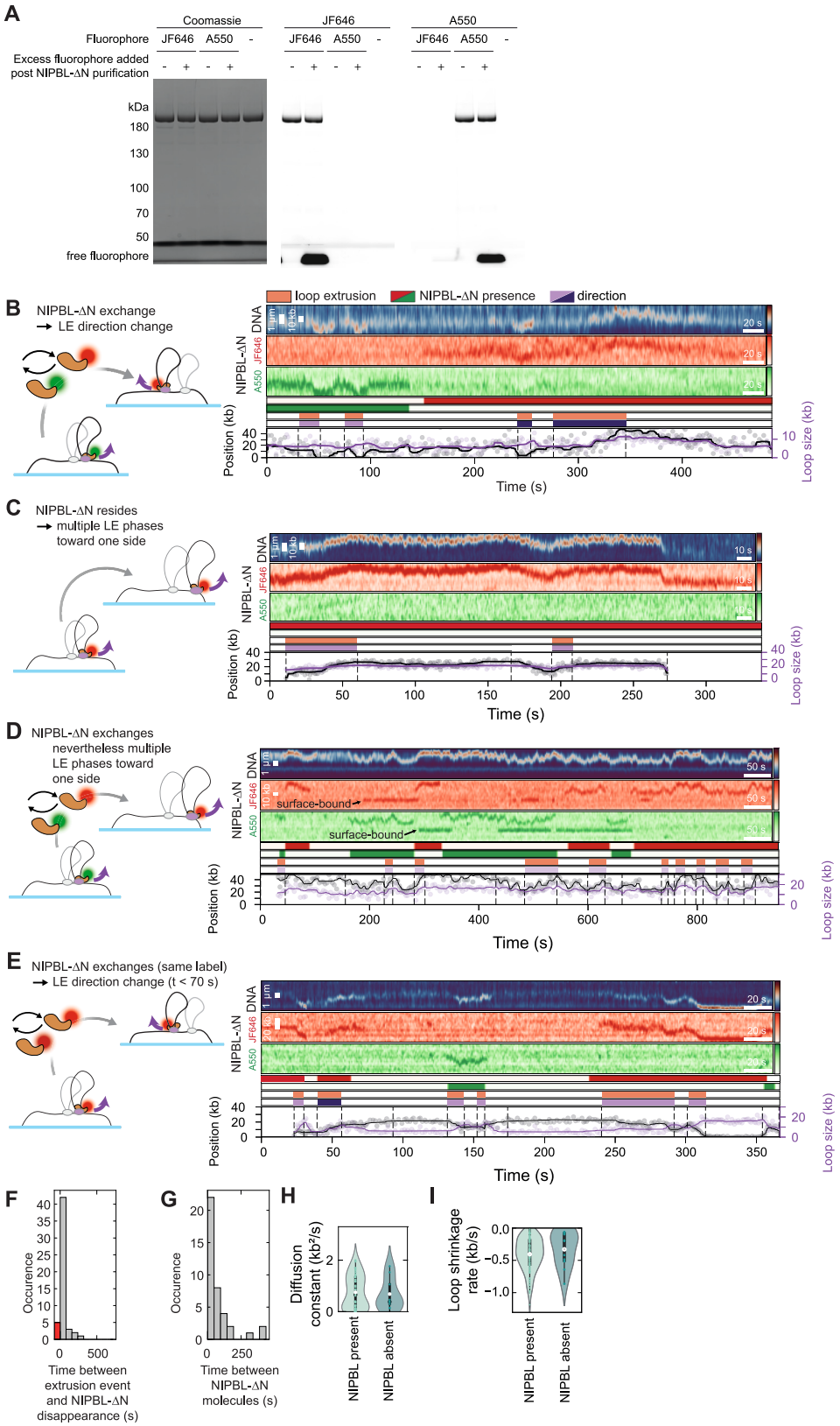

(legend on next page)

Figure S5. Additional loop extrusion traces with differentially labeled NIPBL-ΔN, related to Figure 3

(A) Purity and labeling of NIPBL-ΔN with JF646 and ATTO550, respectively. Molecular weights are indicated in kilodaltons (kDa). An excess of dye was added to the second and fourth lane, respectively, to check whether further labeling can be achieved.

(B) Example trace where cohesin core complex associated with an A550-labeled NIPBL-ΔN first extrudes downward. Upon exchange to a JF646-labeled NIPBL-ΔN at ∼150 s, the cohesin complex extrudes upward (NIPBL-ΔN:cohesin ratio 0.1, 25 mM NaCl). Dots represent raw data, solid lines represent a smoothed version using a Savitzky-Golay filter with window length of 5 s and order 1 (STAR Methods).

(C) Example trace where a JF646-labeled NIPBL-ΔN resides at cohesin, which extrudes solely unidirectionally (here toward the upper end; NIPBL-ΔN:cohesin ratio 0.1, 25 mM NaCl) as in (B).

(D) Example of DNA loop extrusion with exchange of NIPBL-ΔN without direction switch as in (B).

(E) Example of DNA loop extrusion as in (B) with exchange of NIPBL-ΔN and concomitant direction switch between ∼45 and ∼125 s. Another NIPBL-ΔN exchange occurs at ∼240 s but the direction remains (downward here; NIPBL-ΔN:cohesin ratio 0.1, 25 mM NaCl).

(F) Distribution of the time interval between NIPBL-ΔN disappearance and the end of the preceding extrusion phase ($N = 45$; NIPBL-ΔN:cohesin ratio 0.1, 25 mM NaCl). NIPBL-ΔN disappearance coincided with the end of an extrusion event.

(G) Distribution of time between disappearance of one and appearance of the next NIPBL-ΔN molecule ($N = 34$; NIPBL-ΔN:cohesin ratio 0.1, 25 mM NaCl).

(H) Diffusion constant of the DNA loop for diffusion phases in the presence ($N = 36$) and absence ($N = 9$) of NIPBL-ΔN (NIPBL-ΔN:cohesin ratio 0.1, 25 mM NaCl). White dots denote median values, the box extends between the first and third quartile, and whiskers extend to 1.5 × IQR. Statistical significance was assessed by a Mann-Whitney test (not significant $p > 0.05$).

(I) Loop shrinkage rate in the presence ($N = 109$) and absence ($N = 11$) of NIPBL-ΔN (NIPBL-ΔN:cohesin ratio 0.1, 25 mM NaCl). White dots denote median values, the box extends between first and third quartile, and whiskers extend to 1.5 × IQR. Statistical significance was assessed by a Mann-Whitney test (not significant $p > 0.05$).

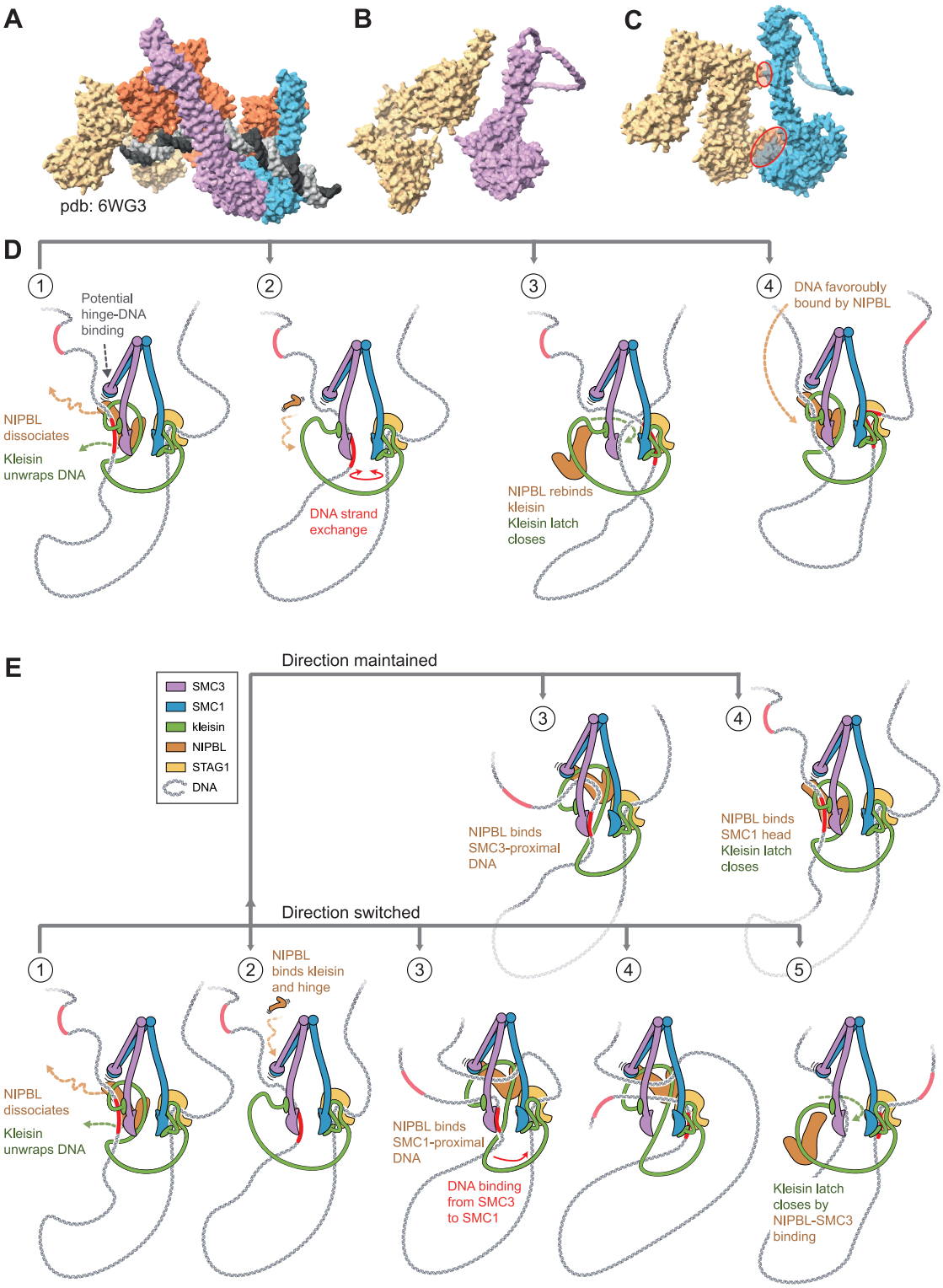

Figure S6. Potential pathways of loop extrusion direction switch via DNA strand exchange mediated by NIPBL exchange, related to Figure 5

(A) Experimentally solved structure of the cohesin-NIPBL-DNA complex in the engaged state (PDB: 6WG3, Shi et al.[42]).

(B) AlphaFold2 prediction of the SMC3 head domain, including a part of the coiled coils (connected by a 64× G linker) and STAG1. No interaction is apparent. Kleisin was included during the folding but is not shown for clarity.

(legend continued on next page)

(C) AlphaFold2 prediction of the SMC1 head domain, including a part of the coiled coils (connected by a 64× G linker) and STAG1. Interactions between STAG1 and SMC1 are apparent close to DNA-binding patches 1 and 2, which were identified by Bauer et al.[41] Kleisin was included during the folding but is not shown for clarity.
(D) Upon dissociation of NIPBL, the kleisin unwraps DNA (step 1). To prevent loss of the SMC3-proximal DNA (red), the SMC3 ATPase head or the SMC hinge may bind DNA. DNA may unbind from STAG1-kleisin concomitantly (step 2). DNA strand exchange may occur spontaneously between the ATPase heads (step 2). Upon rebinding of NIPBL to kleisin (step 3) and closing of the kleisin latch, the former SMC1-proximal strand is poised for the next loop extrusion cycle (step 4).
(E) Step 1 is as described in (D). Alternatively, for the pathway sketched in (A), NIPBL may re-bind the cohesin complex by binding to kleisin and the SMC hinge (step 2). The NIPBL-kleisin-hinge complex may bind either DNA strand that is the one on which loop extrusion subsequently proceeds. If the former SMC1-proximal DNA strand is chosen (step 3, lower), the SMC3-proximal DNA strand exchanges to the DNA-binding site at the SMC1 ATPase head or at STAG1 (steps 3 and 4, lower). If the SMC3-proximal strand is chosen (step 3, upper), no direction switch occurs. The binding of NIPBL-kleisin to the SMC3 ATPase head prepares the complex for the next loop extrusion cycle (step 5, lower; step 4, upper).